IMAGE: A MAP OF THE STARS OF THE ORION CONSTELLATION

Print ISSN: 2631-8490 Online ISSN: 2631-8504

JournalPreview

London Journal of Research in Science: Natural and Formal
Volume 22 | Issue 10 | Compilation 1.0

London Journals Press

WWW.JOURNALSPRESS.COM

LONDON JOURANALS OF RESEARCH IN SCIENCE: NATURAL AND FORMAL

Journal Content
In this Issue

London Journals Press

Iceberg Motion in the Gerlache Strait

Serguei Lonin

ABSTRACT

The First Colombian Scientific Expedition to the Antarctic was carried out during the summer period of the South Hemisphere (January-February 2015) in the Gerlache Strait located by the Antarctic Peninsula. One of the most important investigation tasks during the expedition was the need of having a short-term forecast system of icebergs' trajectories which would help to improve navigation safety for tourist and oceanographic vessels in the region. This paper characterizes the main mechanisms of iceberg's motion, their mathematical representation, and discusses some possible improvements to the way that iceberg dynamics are described.

Keywords: gerlache strait; hydrodynamic model; icebergs.

Classification: DDC Code: 910.09163 LCC Code: G530

Language: English

London
Journals Press

LJP Copyright ID: 925641
Print ISSN: 2631-8490
Online ISSN: 2631-8504

London Journal of Research in Science: Natural and Formal

Volume 22 | Issue 10 | Compilation 1.0

Iceberg Motion in the Gerlache Strait

Serguei Lonin

ABSTRACT

The First Colombian Scientific Expedition to the Antarctic was carried out during the summer period of the South Hemisphere (January-February 2015) in the Gerlache Strait located by the Antarctic Peninsula. One of the most important investigation tasks during the expedition was the need of having a short-term forecast system of icebergs' trajectories which would help to improve navigation safety for tourist and oceanographic vessels in the region. This paper characterizes the main mechanisms of iceberg's motion, their mathematical representation, and discusses some possible improvements to the way that iceberg dynamics are described.

Keywords: gerlache strait; hydrodynamic model; icebergs.

Author: Escuela Naval de Cadetes "Almirante Padilla"; Isla Naval Manzanillo, Cartagena de Indias, Colombia. e-mail: slonin@costa.net.co

I. INTRODUCTION

Iceberg motion is a broad topic that includes the description of its hazards to shipping (Strübing, 1974) and petroleum offshore facilities (Smith & Donaldson, 1987), their potential of becoming large scale water supplies in regions of water-shortage (Job, 1977), and for being natural tracers for marine circulation studies (Garrett et al., 1985a) and climate change assessments.

The state-of-the-art concerning the modelling of icebergs trajectories has three basic approaches. The first one are dynamic, or deterministic, models (e.g. Mountain, 1980; Smith & Banke, 1983; Banke & Smith, 1984; Sodhi & El-Tahan, 1980), which focus on the balance of forces according to the 2nd law of Newton. The second approach uses statistical models (e.g. Garrett, 1984, 1985; Garrett et al., 1985a,b; Gaskill & Rochester, 1984) that are based on statistical properties determined by previously observed trajectories. Of course, the outputs of such a model are probabilistic zones for an iceberg position. Finally, the third type of models is merely a kinematic one (Garrett et al., 1985a, b; Gaskill & Rochester, 1984) which links iceberg drift, wind, and current vectors all together.

Kinematic models might be employed to predict iceberg motion only for short periods of time with poor precision. On the other hand, statistical models depend entirely on previous observations and can thus become obsolete if there are no solid records on winds, waves, and currents. Hence, the deterministic approach seems to be the most convenient from a mathematical point of view, especially when the aim of the modelling is to predict the position of an individual iceberg at all time for navigation safety.

Colombia, in fulfilling its commitments acquired with the ratification of the Antarctic Treaty (1989), has offered its institutions to contribute to the generation of knowledge on Antarctica which would be achieved through the study of ocean dynamics at the Gerlache Strait for operational purposes (navigation). Therefore, the implementation of a forecasting model to predict ice drifts was proposed.

London Journal of Research in Science: Natural and Formal

The Gerlache Strait (Fig. 1), located by the Antarctic Peninsula, is a system of fiords extending 100-150 km by 40-50 km, approximately, with depths varying regularly between 100 and 1000 m. The tidal regime is mainly semi-diurnal 1.6-2.0 m of range and tidal currents are up to 1 m/s (Lonin, 2015). The wind driven circulation may be important too, while some authors indicate a significant thermohaline circulation in the Strait (Moffat et al., 2007; Zhou et al., 2002, 2006; Amos, 1990).

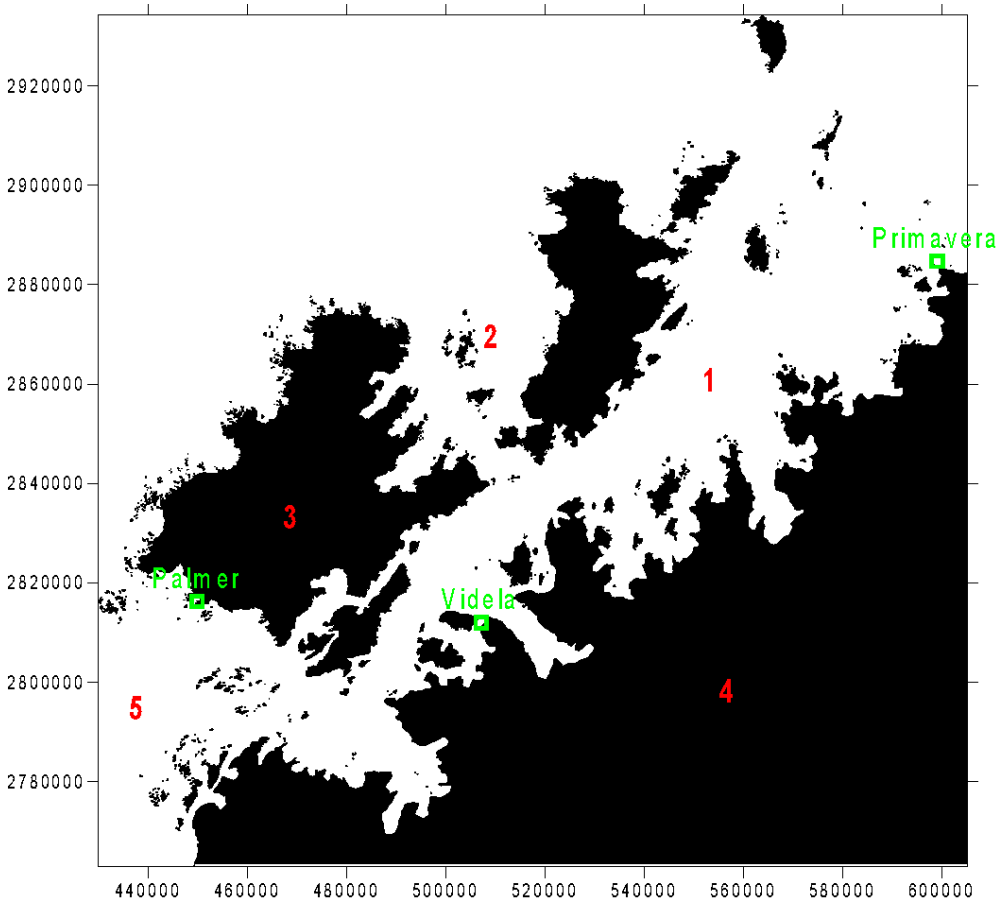

Figure 1: UTM projection of the studied area in the Gerlache Strait). The numbers indicate: 1 – Gerlache Strait; 2 – Schollaert Channel; 3 – Anvers Island; 4 – Antarctic Peninsula; 5 – Bismarck Strait. Stations Primavera (PV), Gerlache Channel (CG) and Palmer (PL) were used to specify the boundary conditions of the sea level (Dragani, et al., 2004).

According to Gladstone *et al.* (2001), iceberg calving is not significant in this part of the Antarctic continent. Nevertheless, local icebergs heading into the Gerlache Strait could be hazardous for navigation.

In the present study, we used the deterministic approach to develop a dynamic model of iceberg motion. Physical and mathematical formulation is presented in the next section. Finally, some relatively important aspects of the model are discussed in Results.

II. MODEL

First, we considered that iceberg thermodynamics can be neglected from the overall dynamics, since the former may be of significant importance only when studying large trajectories (of a few hundred kilometers) for long-term iceberg drifts in which the iceberg´s geometric characteristics change significantly. For such cases, the detailed thermodynamic model may be found in Løset (1993) and Bigg

London Journal of Research in Science: Natural and Formal

et al. (1997). In order to track an individual iceberg along the Gerlache Strait during short-term forecasts (up to 24 hours or much less), for navigation safety purpose, we left as constants the iceberg's mass M, its cross-sectional area A, and a length L of its projection along the water line. The last variable was assumed to be a median value for the range of variations of 1.5:1.0 (observed by Dowdeswell et al., 1992). In other cases, the form of the iceberg might be assumed to be cylindrical with diameter L and a density ratio ρ_i/ρ_w (ice and water density, respectively) proportional to the relationship between their submerged and emerged parts. This allows us to calculate the mass M of an iceberg by estimating the volume of its emerged section with the use of radar.

Second, we have further neglected the effects of iceberg rotation, wave erosion, and sea-ice drag. These assumptions were made due to uncertainties related to the form of any individual iceberg and the difficulties of monitoring or modelling the ice-field properties.

In this simplified case, the principal equations for the lagrangian trajectory of an individual iceberg are:

$$\frac{dX_k}{dt} = < u > + u'_k, \quad \frac{dY_k}{dt} = < v > + v'_k \tag{1}$$

where t is time; <u> and <v> should be defined as components of deterministic velocity of an iceberg in the respective directions x and y, and u'_k and v'_k are oscillation components that may determine the degree of uncertainties of the berg position (X, Y) in space. The index k = 1,..., N is applied when there is more than one lagrangian tracers, introducing statistical uncertainty in the field. Therefore, if N = 1, we should set $u'_k = v'_k = 0$ where such an approach will be fully deterministic. In this case, the principal task is to define the components of <u> and <v>.

Following Bigg *et al.* (1996), the vector of berg motion velocity $\vec{V} = (< u >, < v >)$ may be found from the following equation:

$$M\frac{d\vec{V}}{dt} = -M\vec{f} \times \vec{V} + \vec{F}_a + \vec{F}_w + \vec{F}_r + \vec{F}_p \tag{2}$$

Hereafter, $M\vec{f} \times \vec{V}$ is the Coriolis force; $\vec{F}_a, \vec{F}_w, \vec{F}_r, \vec{F}_p$ are wind, water drags, the wave radiation force, and the horizontal pressure gradient force in the water, correspondingly. Usually, wind and water drags are similarly parametrized in the following form (Bigg, et al., 1996):

$$\vec{F}_x = \frac{1}{2}\rho_x C_x A_x \left|\vec{V}_x - \vec{V}\right|\left(\vec{V}_x - \vec{V}\right), \tag{3}$$

where the subscript x represents air or water; C and A are the respective drag coefficients and cross-section areas of emerged and submerged parts of the berg.

The transition of the radiation stress (S_{ij}) from wind waves to the berg motion should be expressed as a spatial gradient (normal to the berg surface) of the normal stress component $\partial S_{nn}/\partial n$, where

$S_{nn} = \left(2\frac{c_g}{c_f} - \frac{1}{2}\right)E$, given by van Rijn (1994), for mean wave energy density E. The ratio of group velocity and phase velocity $\frac{c_g}{c_f}$ under deep water conditions for short surface waves is equal to 0.5, so the radiation stress would be defined by:

$S_{nn} = \frac{1}{16}\rho_w g H^2$, (H is the wave height; g is gravity).

Multiplying this last expression by L (cross-sectional "effective" length of the berg), the wave radiation force would be given by:

$$\vec{F}_w = S_{nn} L . \tag{4a}$$

This result is identical to the one obtained by Smith (1993):

$$\vec{F}_w = \frac{1}{18}\rho_w g a^2 L \frac{\vec{V}_a}{|\vec{V}_a|}, \text{ (a = H/2; } \vec{V}_a \text{ is the wind vector),} \tag{4b}$$

but may be restricted by shallow-water conditions of the Gerlache Strait and by the differences between wave propagation and local wind direction.

Finally, the pressure gradient force in (2) represents an amount of the hydrodynamic forces and should be calculated directly from a hydrodynamic model. The model employed in this study is an advanced version of MECCA (Hess, 1989), which is based on the system of primitive equations of motion with complete thermodynamics and a sub-model of turbulence:

$$\frac{\partial u}{\partial t} + \frac{\partial u^2}{\partial x} + \frac{\partial uv}{\partial y} + \frac{\partial uw}{\partial z} = -\alpha_0 \frac{\partial P}{\partial x} + fv + \frac{\partial}{\partial x}\left(2A_h \frac{\partial u}{\partial x}\right) + \\ + \frac{\partial}{\partial y}\left(A_h\left[\frac{\partial v}{\partial x} + \frac{\partial u}{\partial y}\right]\right) + \frac{\partial}{\partial z}\left(A_z \frac{\partial u}{\partial z}\right), \tag{5}$$

$$\frac{\partial v}{\partial t} + \frac{\partial uv}{\partial x} + \frac{\partial v^2}{\partial y} + \frac{\partial vw}{\partial z} = -\alpha_0 \frac{\partial P}{\partial y} - fu + \frac{\partial}{\partial y}\left(2A_h \frac{\partial v}{\partial y}\right) + \\ + \frac{\partial}{\partial x}\left(A_h\left[\frac{\partial v}{\partial x} + \frac{\partial u}{\partial y}\right]\right) + \frac{\partial}{\partial z}\left(A_z \frac{\partial v}{\partial z}\right), \tag{6}$$

$$\frac{\partial P}{\partial z} = -\rho g, \tag{7}$$

$$\frac{\partial u}{\partial x}+\frac{\partial v}{\partial y}+\frac{\partial w}{\partial z}=0, \tag{8}$$

$$\rho=\rho_0[1+F_\rho(S,T)] \quad , \tag{9}$$

$$\frac{\partial S}{\partial t}+\frac{\partial uS}{\partial x}+\frac{\partial vS}{\partial y}+\frac{\partial wS}{\partial z}=\frac{\partial}{\partial x}\left(D_h\frac{\partial S}{\partial x}\right)+\frac{\partial}{\partial y}\left(D_h\frac{\partial S}{\partial y}\right)+\frac{\partial}{\partial z}\left(D_z\frac{\partial S}{\partial z}\right), \tag{10}$$

$$\frac{\partial T}{\partial t}+\frac{\partial uT}{\partial x}+\frac{\partial vT}{\partial y}+\frac{\partial wT}{\partial z}=\frac{\partial}{\partial x}\left(D_h\frac{\partial T}{\partial x}\right)+\frac{\partial}{\partial y}\left(D_h\frac{\partial T}{\partial y}\right)+\frac{\partial}{\partial z}\left(D_z\frac{\partial T}{\partial z}\right)+\frac{\partial R}{\partial z}, \tag{11}$$

where u, v, and w are current velocity components in the directions x, y and z, respectively; ($\alpha_o = 1/\rho_w$); A_h and A_z are horizontal and vertical turbulence; D_h and D_z are turbulent diffusion of heat (T) and salt (S), and R is a shortwave specific flux of solar radiation that penetrates the water column below the surface. All other denominations have been already specified above.

The system described by (5-11) is a closed one as boundary conditions were specified (sea level tidal oscillations [data from Dragani, et al., 2004]; temperature and salinity profiles from the First Colombian Scientific Expedition [January-February 2015], turbulence closure at 2.5-level [Mellor & Yamada's hierarchy], heat and impulse fluxes at the sea surface, and interpolated initial thermohaline fields, and cold-start initialization). Bathymetry was collected during the expedition and combined with a GEBCO-0.5 data set (Fig. 2).

Therefore, the pressure gradient force may be found from (5) and (6) as:

$$\vec{F}_w=-\alpha_0 M\left(\frac{\partial P}{\partial x},\frac{\partial P}{\partial y}\right) \tag{12}$$

where the applied force corresponds to both barotropic and baroclinic modes of motion.

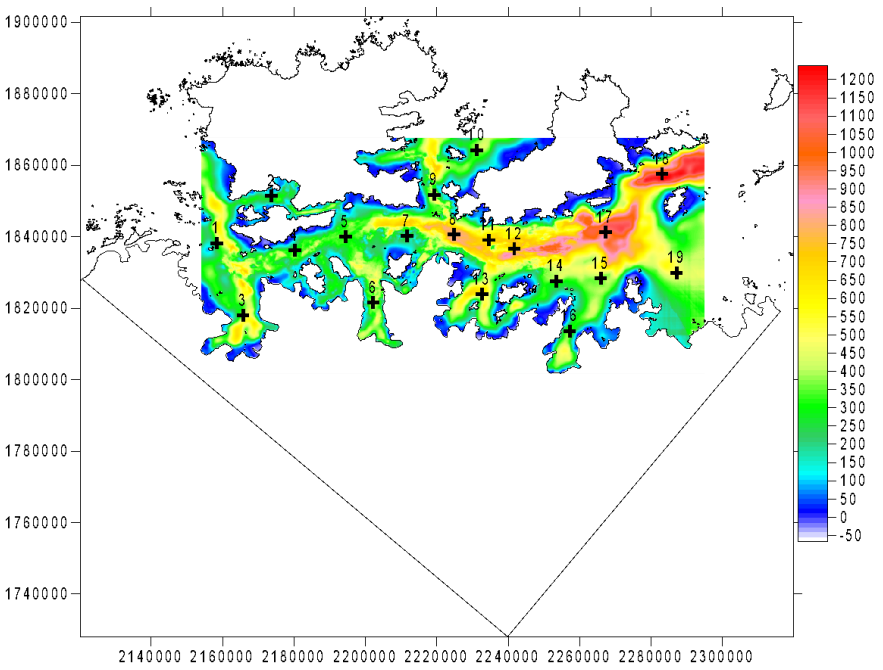

Figure 2: Hybrid bathymetry obtained from hydrographic survey during the First Colombian Scientific Expedition (January-February 2015), combined with GEBCO-0.5. Points 1-19 indicate the initial position of icebergs in numerical experiments. (Domain rotated 40°, Fig. 1)

III. RESULTS AND DISCUSSION

Figures 3 and 4 present spatial ranges of sea-level variations during one half of a semi-diurnal tide period. It seems that along the strait the level spatial differences can achieve up to 20 cm for the amplitude of 80 cm of tide. It conducts high tidal currents about 1 m/s of velocity.

The model simulations of the First Colombian Scientific Expedition demonstrate that the thermohaline circulation contributes up to 40% to the dynamics of the strait. Meanwhile, wind and wave data indicates a weak generation of gravity waves and wind-driven currents. Probably, this is because measurements were taken during a certain period of the year, with occasional local weather conditions.

Figures 5 and 6 show iceberg trajectories as an example of the model outputs.

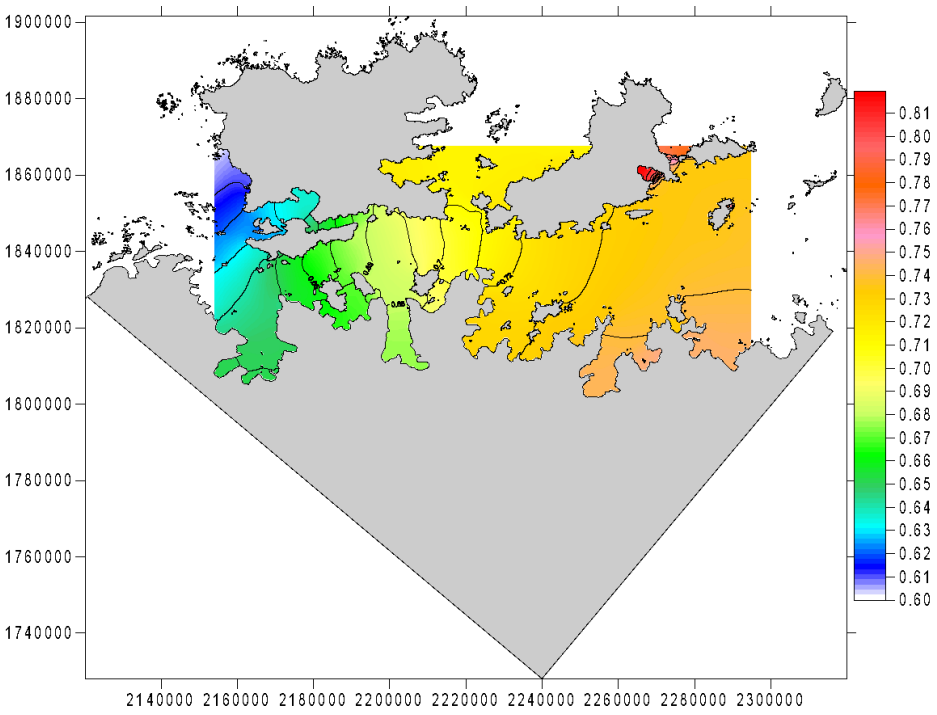

Figure 3: Modeled sea-level field (in m) during the high-water phase of tides

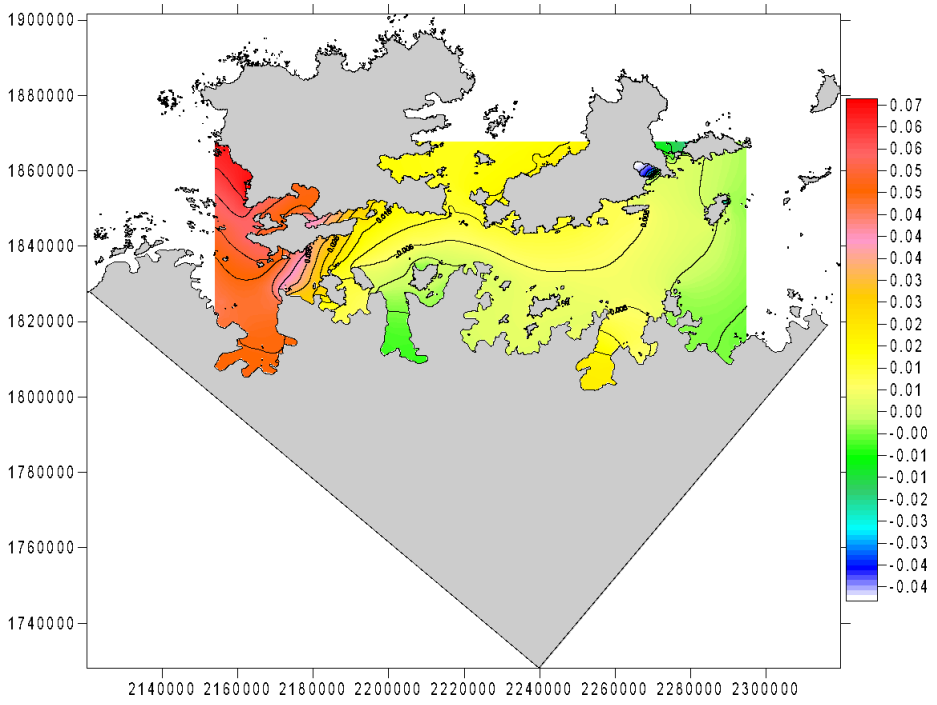

Figure 4: Modeled sea-level field (in m) close to the mean level conditions

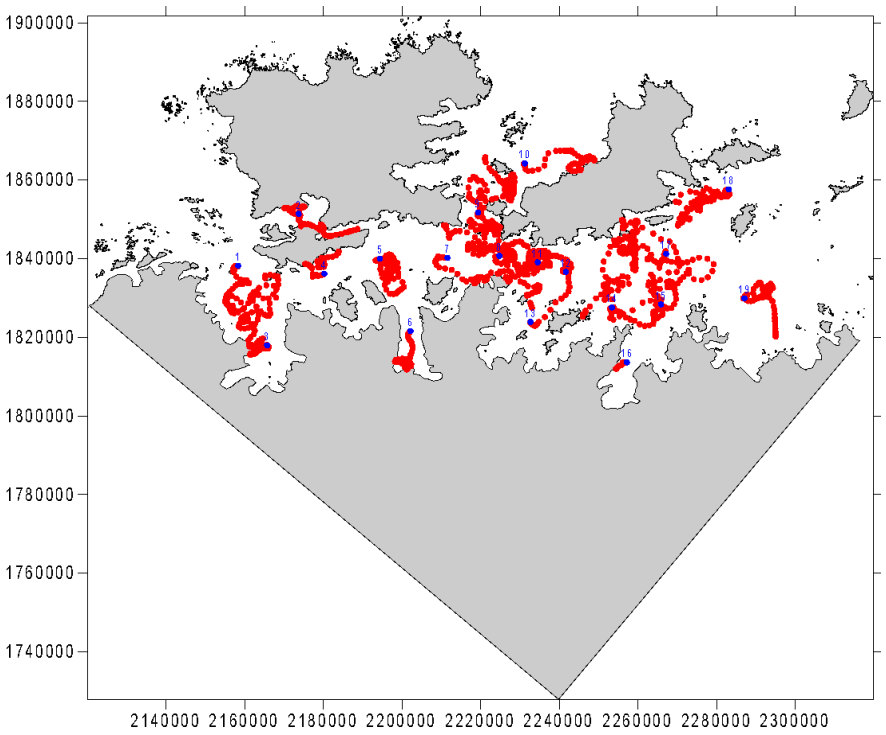

Figure 5: Motion of hypothetic icebergs during four days of simulation. Starting points were indicated in Fig. 2.

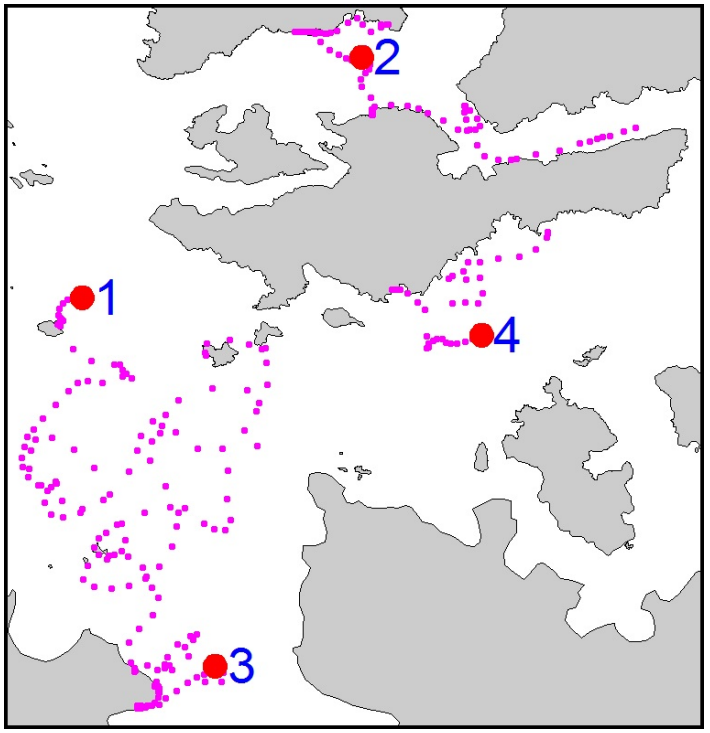

Figure 6: Trajectories of icebergs 1-4 (Fraction of the Fig. 5)

The obtained results correspond to a finite-difference grid of 200 m of resolution. The integration time step was 10 seconds for the hydrodynamic model and 600 seconds for the equations (1) and (2). The

mass of icebergs was selected arbitrarily and simulations were run after achieving cuasi-stationary regime for hot-start initiation.

Some work considerations were elaborated. First of those is related to the fact that geostrophic relationships would not be useful to find currents fields for the balance (2), as in Smith & Banke (1983). This is due to strong oscillatory tidal fluxes in the Gerlache Strait. It is well-known that tidal gravitational modes are very weak in the open oceans and the approximation of Smith & Banke (1983) would be admissible. Moreover, in the majority of previously cited works (e.g. Smith & Donaldson, 1987), the pressure gradients for (2) are found from cuasi-geostrophic equilibrium with the acceleration adjustment [something similar would happen if we would put in (5) and (6) the equilibrium between the first term on the left-hand side, and the first and second terms of the right-hand side of those equations]. The nature of tidal-predominant motion in the Gerlache Strait allows us to think that the use of the complete hydrodynamic model (5)-(11) together with suitable external conditions is the unique alternative to calculate the pressure gradients by (12) and currents fields for (2).

A second aspect can be appreciated. In the principal equation (2) of iceberg motion, the left side of the equation was reported to be relevant only for long-term trajectories (Bigg et al., 1996). Indeed, the Coriolis force in (2) is a secondary one (it doesn't produce work by itself); the oceanic thermohaline variability is really slow [the last term in (2)], while the current drag force (3) in absence of winds and waves "is limited", i.e. it has a limited range of action when there is no presence of mass M of the iceberg. Therefore, for a huge mass value M the "compensatory" acceleration in (2) should be very small, which confirms the conclusions made by Bigg et al. (1996). Due to the tidal-predominant motion, the effect of barotropic mode in the pressure gradient (12) is noticeable at the Gerlache Strait. The effect of "mass compensation" in (2) becomes less important and the acceleration of iceberg should be stronger. Does this mean a better or worse predictability of iceberg trajectories?

The next topic is related to the description of wave stress forces. Given by (4), there are at least two clarifications that must be made: a) For relatively shallow water (not deep-water conditions for the wind waves), should the wave radiation force be sub-estimated until an iceberg achieves a certain depth and gets grounded? And, b) The factor L is rather arbitrary, depends on the form of the berg. Hence, diffraction effects and other components of wave stress (not only normal to its frontal side) should be estimated.

IV. CONCLUSIONS

The present work was a first attempt to describe iceberg dynamics, based on studies about the physics of mechanisms of its motion, known for large scales and long terms. The majority of the forces are parametrizations.

The Gerlache Strait is a rigid hyperbolic system with tidal predominance. So, it was demonstrated that one of the principal forces affecting icebergs (pressure gradient in water) should be sought directly from the primitive hydrodynamic equations.

Nevertheless, it seems that the main error in the trajectory prediction is related to precision of mass estimation and geometrical parameters of icebergs. The bigger the iceberg, the lesser the acceleration it suffers. The acceleration, therefore, becomes a sensitive factor of the drift. One can suppose that under tidal-predominant conditions, this kind of error should be smaller.

ACKNOLEDGEMENTS

This work was supported by contract number 096-GINRED4-15 of the General Maritime Agency (DIMAR) of Colombia. The hydrographic and oceanographic data was collected during the First Colombian Scientific Expedition to the Antarctic (January-February 2015).

REFERENCES

1. Amos, A. (1990): RACER: Meteorological conditions during the spring bloom in the Gerlache Strait. *Antarctic Journal of the United States*. pp. 128-131.
2. Banke, E.G. and S.D. Smith. (1984). A Hindcast Study of Iceberg Drift on the Labrador Coast. *Can. Tech. Rep. Hydrogr. Ocean Sci.* 49, 161 p.
3. Bigg, G.R., M.R. Wadley, D.P. Stevens, and J.A. Johnson (1996). Prediction of iceberg trajectories for the North Atlantic and Arctic Oceans. *Geophys. Res. Letters*, Vol. 23, No. 24, pp. 3587-3590.
4. Bigg, G.R., M.R. Wadley, D.P. Stevens, and J.A. Johnson (1997). Modelling the dynamics and thermodynamics of icebergs. *Cold Regions Science and Technology*, 26, pp. 113-135.
5. Dragani W.C., M.R. Drabble, E.E. D'Onofrio & C.A. Mazio. (2004). Propagation and amplification of tide at the Bransfield and Gerlache Straits, northwestern Antarctic Peninsula. Polar Geosci., 17, pp. 156-170.
6. Garrett, C.J .R, (1984). Statistical prediction of iceberg trajectories. *Iceberg Research*, 1, 7, pp. 3-7.
7. Garrett, C.J.R. (1985). Statistical prediction of iceberg trajectories. *Cold Regions Sci. Technol.*, 11, pp. 255-266.
8. Garrett, C.J.R., J . Middleton, M. Hazen and F. Majaess. (1985a). Tidal currents and eddy statistics from iceberg trajectories off Labrador. *Science*, 227, 1333-1335.
9. Garrett, C.J.R., J.F. Middleton, F. Majaessand M. Hazen. (1985b). Analysis and prediction of iceberg trajectories. *Internal Report, Dept. of Oceanography*. Dalhousie University, 86 pp.
10. Gaskill, H.S. and J. Rochester. (1984). A new technique for iceberg drift prediction. *Cold Regions Sci. Technol.*, 8, pp. 223-234.
11. Gladstone, R.M., G.R. Bigg and K.W. Nickolls (2001). Iceberg trajectory modeling and meltwater injection in the Southern Ocean. *J. Geophys. Res.*, Vol. 106, No. C9, pp. 19.903-19.915.
12. Hess, K.W. (1989). MECCA Programs Documentation. NESDIS, NOAA.
13. Job, J.G. (1977). Moving Unprotected Icebergs to Southern Continents. In: *Proceedings of the First International Conference and Workshops on Iceberg Utilization for Fresh Water Production, Weather Modification and Other Applications*. Iowa State University, Ames, Iowa, USA, October 2-6, 1977.
14. Lonin, S. (2015). A hydrodynamic model of Gerlache Strait (Antarctic) during summer of the Southern Hemisphere. *Boletín Científico CIOH*, No. 33, pp. 145-167 (ISSN: 0120-0542).
15. Løset, S. (1993). Thermal energy conservation in icebergs and tracking by temperature. *J. Geophys. Res.*, 98, pp. 10.001-10.012.
16. Moffat, C., R. Beardsley, Owens, B. & Van Lipzig, N. (2007). A first description of the Antarctic Peninsula Coastal Current. Deep Research II 55. pp. 277-293.
17. Mountain, D.C. (1980). On predicting iceberg drift. *Cold Regions Sci. Tech.*, 1, pp. 273-282.
18. Smith, S.,D., and N.R. Donaldson (1987). Dynamic modelling of iceberg drift using current profiles. *Canadian Tech. Rep. of Hydrography and Ocean Sciences* No. 91
19. Smith, S.D and E.G. Banke. (1983). The influence of winds. currents and towing force on the drift. of icebergs. *Cold Regions Sci. Technol.* 6, pp. 241 -245.
20. Smith, S.D. (1993). Hindcasting iceberg drift using current profiles and winds. *Cold Regions Science and Technology*, 22, pp. 33-45.
21. Sodhi, D.S. and M. EI-Taban. (1980). Prediction of an iceberg drift trajectory during a storm. *Ann. Glaciol.*, 1, pp. 77-82.

22. Strübing, K. (1974). Eisberge im Nordatlantil – 60 Jahre International Ice Patrol. *Der Wetterlotse*, 26, pp. 141-160.
23. Van Rijn, L.C. (1994). Principles of Fluid Flow and Surface Waves in Rivers, Estuaries, Seas and Oceans. *Aqua Publ.*, The Netherlands.
24. Zhou, M., P. Niilerb, & Hu, J-H. (2002). Surface currents in the Bransfield and Gerlache Straits, Antarctica. Deep Sea Research Part I: Oceanographic Research Papers, 49 (2002) pp. 267–280.
25. Zhou, M., P. Niilerb, Zhua, Y. & Dorlanda, R. (2006). The western boundary current in the Bransfield Strait, Antarctica. Deep Sea Research Part I: Oceanographic Research Papers Volume 53, Issue 7, July 2006, pp. 1244–1252.

This page is intentionally left blank

Obscuring Torus in AGN as a Vortex in the Radiation Flux and its Influence on the Determined Masses of Super Massive Black Holes

V.M. Kontorovich

ABSTRACT

The influence of the radiation flux from the accretion disk on obscuring tori in active galactic nuclei and the inverse effect of torus gravity on the disk and the position of the region of broad emission lines are considered. It is shown that the latter can affect the values of masses of supermassive black holes in the centers of galaxies determined by the reverberation method.

Keywords: AGN, SMBH, obscuring (shading) torus, radiation flux, eddington luminosity, twisting torus by radiation, streamlines (topology of), lagrange ring, reverberation mapping.

Classification: DDC Code: 523.1 LCC Code: QB981

Language: English

London Journals Press

LJP Copyright ID: 925642
Print ISSN: 2631-8490
Online ISSN: 2631-8504

London Journal of Research in Science: Natural and Formal

Volume 22 | Issue 10 | Compilation 1.0

Obscuring Torus in AGN as a Vortex in the Radiation Flux and its Influence on the Determined Masses of Super Massive Black Holes

V.M. Kontorovich

ABSTRACT

The influence of the radiation flux from the accretion disk on obscuring tori in active galactic nuclei and the inverse effect of torus gravity on the disk and the position of the region of broad emission lines are considered. It is shown that the latter can affect the values of masses of supermassive black holes in the centers of galaxies determined by the reverberation method.

Keywords: AGN, SMBH, obscuring (shading) torus, radiation flux, eddington luminosity, twisting torus by radiation, streamlines (topology of), lagrange ring, reverberation mapping.

Author: Radio Astronomy Institute NAS of Ukraine, Kharkiv.

I. INTRODUCTION. OBSCURING TORUS IN AGN

Active galactic nuclei (AGNs, see reviews [1 ,2]), responsible for the phenomenon of quasars and radio galaxies (RGs), as well as less powerful but more numerous Seyfert galaxies (Sy I and Sy II), apparently have a universal structure [3,4] and contain a supermassive black hole (SMBH, Lynden-Bell, 1969; see revs[5-7]), an accretion disk [8-9], outflowing plasma flows in the form of jets [10-12] and wind [13], and obscuring (shading) tori (ST, [3]). The latter serve as accumulators and regulators of the accreting matter and, most likely, represent grandiose self-gravitating vortices with peculiar dynamics [14]. The observed pattern of AGN depends on the orientation of the line of sight relative to the axis of the torus. When the axes are oriented close to parallel, the inner part of the AGN with broad emission lines (Sy I, quasars) is visible. If the axes are not substantially parallel and the torus obscures the central region of the nucleus, broad lines are not visible in direct radiation (Sy II, RG), but may appear in polarized light scattered by the corona [3] (see also Urry & Padovani 1995 for RGs).

It is significant that AGN together with ST represent a self-consistent system where strong gravitation, powerful radiation at a level close to the Eddington limit [15], and a peculiar vortex dynamics of ST, which is responsible for the self-consistency of the accretion and emission processes, as well as for a number of observables interacting effects in AGN. These include, in particular, bursts of radiation, correlating with emissions of superluminal components of radio jets [16].

II. ORIGIN AND PROPERTIES OF ST

The gas and dust torus is a component and result of the power accretion of matter onto the SMBH. The accretion flow itself, apparently, arises as a result of a collision or merger of galaxies [17,18]. The latter are the main reason for the emergence of massive galaxies and SMBHs at their centers [1]. Mass growth as a result of mergers formally to infinite mass is explosive [19-20] , and according to the solutions of the kinetic coagulation equation (Smoluchowski's equation) [18], is formed in a finite time. This

[1] In the Early Universe, with a deficit of heavy elements, other scenarios for the formation of massive objects are possible, related to the features of star formation under these conditions.

requires that the merger probability grows faster than the first power of the mass, which is exactly what happens in the case of gravitational interactions.[2]

The accretion disk, which is an extremely efficient converter of gravitational energy into radiation (Ya.B. Zeldovich, E. Salpeter), is formed in close proximity to the BH, starting from the boundary of stable orbits, and extends to scales of 0.01-0.1 ps [9]. The disk heats up due to the friction of neighboring layers and its thermal radiation, which is proportional to the BH mass growth rate, is limited by the Eddington limit [15], at which the radiation pressure makes it impossible for the substance to fall further onto the center. Due to the fact that the disk radiation, according to Lambert's law [21,22], is non-isotropic and mainly directed along the normal to the disk plane, where it can exceed the Eddington limit, a hollow cone free of resting matter is formed above the disk. Outside this cone, the disk radiation intensity is less than the Eddington one, as a result of which STs are formed (Fig. 1). But there is also no direct fall of matter on the center outside the cone. A torus is a (gravitational) attractor [23], around the central generatrix of which matter moves in closed orbits, forming a toroidal vortex [14]. And only a small part of this matter rotating around the toroidal attractor gets to the center and "feeds" the accretion disk [14, 24-25].

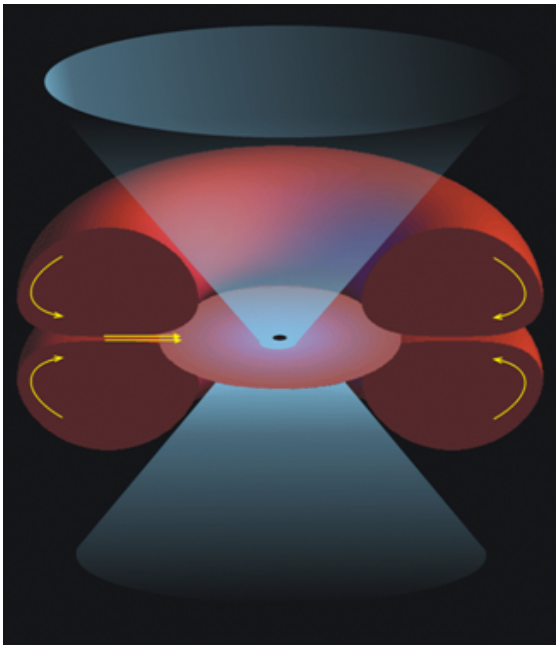

Fig.1. Diagram explaining the AGN model used. The SMBH is shown at the center of symmetry, the accretion disk in the (x-y) plane, the cone of wind and radiation from the accretion disk, the obscuring torus twisted by wind and radiation, and the streamlines inside the ST [14, Bannikova, Kontorovich, 2007].

Not shown: jets, scattering corona, accretion disk wind.

The plane of the accretion disk is a mirror plane of symmetry for the torus, resulting in a characteristic "dipole" structure of streamlines, where the "top" and "bottom" parts of the vortex rotate in opposite directions. The simplest example of such a topology can be the streamlines in the flow around a liquid cylinder [26], where the "twisting" of the substance inside the cylinder is carried out by the flow around (Fig. 2). The same topological pattern of streamlines is realized in the meridional section of the Hill vortex [27], in the Larichev-Reznik soliton [28], and other similar examples. In AGN, the corresponding "twisting" is carried out by the radiation flux from the accretion disk [14], partially "flowing around" the torus, and partially absorbed by the surface of the torus.

[2] The accelerated expansion of the Universe could put an end to this process and thus determine both the maximum mass of galaxies and the SMBH at their centers.

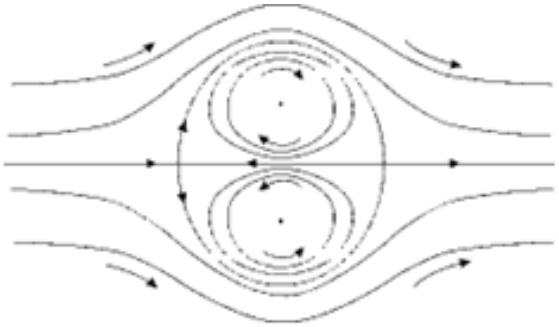

Fig.2: Topological structure of streamlines of matter and radiation similar to ones in the shading torus near AGN center: right side is the x-z section by a plane of symmetry orthogonal to the disk (left, not shown); z-axis is the axis of symmetry. The arrows show possible motions of matter in the torus and in flow around it, corresponding to the solution of the flat problem of a flow around a cylinder [14,25].

We simplify the description by replacing a small part of the torus with a large radius *R* with a circular cylinder of the same cross section with radius *a*. The angular dependence of the radiation intensity on the polar angle ϑ (with the polar axis orthogonal to the plane of the accretion disk) will be chosen in accordance with the Lambert law [22-23] in the form $I(\vartheta) = I_{\max} \cos\vartheta$. In this case, the total luminosity $L = 2 \cdot 2\pi \int_0^{\pi/2} d\vartheta \cdot I(\vartheta) = 4\pi I_{\max}$. The power of the direct radiation of the disk [3], which is not covered by the torus, is equal to $W = 4\pi \cdot \int_0^{\theta} d\vartheta \cdot I(\vartheta) = L \cdot \sin\theta$, where on the beam tangent to the surface of the torus $\vartheta = \theta$, the intensity is locally equal to the Eddington intensity: $I_{Edd} = L_{Edd} / 4\pi = I(\theta)$, $L_{Edd} \approx 1{,}5 \cdot 10^{38} M_c / M_\odot$ erg/sec. Here M_c is the mass of the SMBH and $M_\odot$ is the mass of the Sun. The foregoing requires reservations and clarifications, some of which will be explained below. The terminology used implies that the size of the disk is much smaller than the larger radius of the torus *R*, due to which the disk can be considered as a point emitter coinciding with the center of symmetry of the system, but non isotropic (according to Lambert's law) emitter.

The opening angle of the hollow cone is determined by the excess of the maximum intensity over the Eddington one:

$$\cos\theta = \frac{I_{Edd}}{I_{\max}} \quad (2.1)$$

Accordingly, with an increase in the AGN power (with some reservations), the degree of coverage of the emitting region of the ST should decrease, which, apparently, is observed according to [29] regardless of the internal structure of the torus (clamps or a continuous medium).

[3] Torus, whose temperature is much lower than the temperature of the disk, re-radiates the absorbed energy of hard radiation of the disk in the low-frequency (IR) range, which we do not take into account in these considerations. We also do not take into account the polarized radiation scattered by the AGN "corona".

III. VORTEX DYNAMICS OF AN OBSCURING TORUS

As is known [26-27, 30], the equation for the stream function ψ, $\Delta\psi = f(\psi)$, where the components of the plane flow velocity are:

$$V_x = \frac{\partial\psi}{\partial z}, \quad V_z = -\frac{\partial\psi}{\partial x}, \tag{3.1}$$

for $f(\psi) = -k^2\psi$ in polar coordinates $x = r\cdot\cos\beta$, $z = r\cdot\sin\beta$ becomes [25]:

$$\frac{\partial^2\psi}{\partial r^2} + \frac{1}{r}\frac{\partial\psi}{\partial r} + \frac{1}{r^2}\frac{\partial^2\psi}{\partial\beta^2} + k^2\psi = 0 \tag{3.2}$$

Its solution inside the circle $\psi = CJ_1(kr)\sin\beta$ at $J_1(ka) = 0$, where J_1 is the first-order Bessel function, a is the radius of the cylinder in a stream, is conjugated with the solution outside the circle $\psi = U\cdot\left(r - \frac{a^2}{r}\right)\cdot\sin\beta$, because the values of the stream function and the tangential velocity on both sides of the boundary $r = a$ coincide. This can be easily verified using the relationship of the velocity components $r\frac{d\beta}{dt} = V_\beta$, $\frac{dr}{dt} = V_r$, with the current function $\psi(r,\beta)$, which in polar coordinates takes the form:

$$V_\beta = -\frac{\partial\psi}{\partial r}, \quad V_r = \frac{1}{r}\frac{\partial\psi}{\partial\beta}. \tag{3.3}$$

It is easy to verify the latter by making the change of variables in expressions (3.1) with the help of the Jacobians

$$\frac{\partial(z,x)}{\partial(r,\beta)} = -r, \frac{\partial(\psi,x)}{\partial(z,x)} = -\frac{1}{r}\frac{\partial(\psi,x)}{\partial(r,\beta)}, \frac{\partial(\psi,z)}{\partial(x,z)} = \frac{1}{r}\frac{\partial(\psi,z)}{\partial(r,\beta)},$$

$$\frac{\partial(\psi,z)}{\partial(r,\beta)} = \frac{\partial\psi}{\partial r}\frac{\partial z}{\partial\beta} - \frac{\partial\psi}{\partial\beta}\frac{\partial z}{\partial r}, \frac{\partial(\psi,x)}{\partial(r,\beta)} = \frac{\partial\psi}{\partial r}\frac{\partial x}{\partial\beta} - \frac{\partial\psi}{\partial\beta}\frac{\partial x}{\partial r}. \tag{3.4}$$

As a result, [25] we get the value for the constant $C = \frac{2U}{kJ_1'(ka)} = -\frac{2U}{kJ_0(ka)}$, where the value $ka \approx 1,2\pi$ corresponds to the smallest root of the Bessel function J_1.

IV. RADIATION FLOW AROUND

The picture of the "flow around" the radiation flux differs significantly due to the absorption of the ST radiation and its separation on the streamline corresponding to the Eddington intensity. But inside the

torus, the topology of streamlines remains the same as in the problem of flow around a cylinder (Fig. 3).

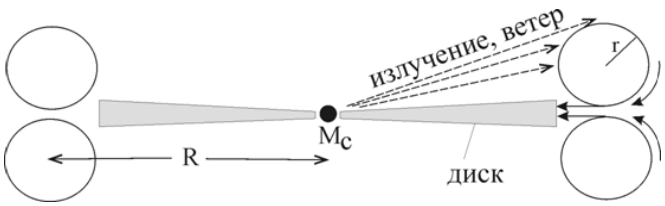

Fig.3. Scheme of "twisting" the ST by the wind and AGN radiation. External and internal critical power lines are not Shown to highlight the dipole structure torus, consisting of two counter rotating ring vortices [14,25,].

Fig.3

The beam of field lines corresponding to the Eddington radiation intensity transmits the tangential momentum of the torus surface at the point of contact at $\vartheta = \theta$. Let us find the speed of the matter of the torus at this point, using the law of conservation of momentum, which takes the form of continuity of the momentum flux when radiation is absorbed by the shading torus. The flux density of the radiation pulse on the beam of rays of interest to us, corresponding to the Eddington intensity, is equal to

$$\frac{J(\theta)}{c} = \frac{L_{Edd}}{4\pi c\left(R^2 - a^2\right)\sin\theta} \tag{4.1}$$

Here, the distance to the point of contact of the beam is $r = \sqrt{R^2 - a^2}$, where R is the large radius of the torus - the distance to the central generatrix of the torus, counted from the center of the AGN (i.e., from the SMBH), a is the small radius of the torus.

The flux density of the tangential component of the momentum in the torus at the point of contact is [30]

$$\Pi_{tt} = \rho V_t^2 + p \,, \tag{4.2}$$

where ρ is the density of the torus, V_t is the tangential velocity, and the contribution of pressure in a relatively cold torus can be neglected.

Equating (4.1) and (4.2), we find for the tangential velocity component

$$V_t = \sqrt{\frac{L_{Edd}}{4\pi\rho c\left(R^2 - a^2\right)\sin\theta}} \tag{4.3}$$

We do not take into account the influence of the wind, but since the wind itself is a product of the radiation flux, this should not significantly affect the estimates obtained. However, the pattern of the wind streamlines near the torus should differ from rectilinear rays (Fig. 3) and, rather, will approach the pattern of flow around the material cylinder (Fig. 2). At the same time, from the condition of continuity of the tangential velocity at the point of contact of the rays $\pi - \beta = \theta$ (the equality of angles with mutually orthogonal sides was used), we find:

$$U = \sqrt{\frac{L_{Edd}}{16\pi\rho c\left(R^2 - a^2\right)\sin^3\theta}}. \qquad (4.4)$$

After that, you can use the solution formulas for the flow around the cylinder.

Thus, the radiation and the wind carry a "twist" transforming ST to a vortex. Another limiting case when the vortex is formed by initial conditions, as for example colligion or merging galaxies, see in connection of Hoag's object theory in [31].

V. INSTABILITY OF THE ACCRETION DISK PERIPHERY AND BLR IN AGN

The presence of massive STs leads to competition between two gravitational attractors: SMBH and ST. At least in the plane of the disk, this leads to the appearance of an instability region near the so-called Lagrange rings (LR) [32,33]. LR is a generalization of the interior Lagrange point for a test particle in the restricted three-body problem for the case when, along with the SMBH, the second body is a massive self-gravitating body – a torus or a massive ring. If we confine ourselves to the potential of a thin torus, it is not difficult to obtain a relationship between the mass ratio of the torus and the BH and the position of the Lagrange ring. In this consideration, we will assume that the region of broad BLR emission lines near the LR is a manifestation of the instability region. This idea is supported by the flat structure of this region observed in some cases [1, 2] and the appearance of double lines, which may be a consequence of the Keplerian rotation [4]. This representation is only an assumption [4] that needs additional observational justification. However, some conclusions that are important for the method of determining the SMBH masses by the widely used reverberation method [1, 2, 34] can follow from this.

At present, even the largest optical and IR interferometers do not have enough spatial resolution to observe (with few exceptions in the nearby Seyfert galaxies) a region of broad emission lines. But the temporal resolution turns out to be sufficient (J.Bacal) to determine the distance to the manifestation of this burst in the BLR lines [34-37] from the delay of the moment of the burst of fluctuations in the continuous spectrum of the disk emission. In this case, using the virial relations in the gravitational field of the SMBH and the measured linewidths, the BH masses at the AGN centers are determined according to $M_c = c\tau \cdot \left(\Delta V\right)^2 \cdot G^{-1}$, where the virial coefficient of the order of one-two [1,2] also appears, determined from statistical considerations. The influence of the gravitational field of the ST can significantly affect the form of this relation and, thus, the mass of the black hole determined with its help [5]. Note that for a thin torus, the position of the Lagrange Ring, near which BLR can be expected, is determined by the ratio of the masses of the SMBH and ST according to [32, 33]

$$\frac{M_c}{M_{ring}} = \frac{q}{\pi(1-q^2)}\left[(1+q)E\left(k\right) - (1-q)K\left(k\right)\right], \quad k^2 = 4q/\left(\left(1+q\right)^2 + z^2\right), \qquad (5.1)$$

[4] Another popular assumption is that BLRs are a system of clouds falling on the center or dispersed by light pressure and wind from the center encounters the difficulty consisting in the absence of an observed analogue of the shot effect.

[5] The Influence of attraction to the torus on the tangential component of the velocity near the point of tangency of the beam in this consideration can be neglected, since this force is directed approximately along the normal.

where $E(k)$ and $K(k)$ are complete elliptic integrals, k is their index, and the dimensionless lengths are measured in units of the large torus radius R.

In the general case, the virial relation for determining the mass of the SMBH should also include the mass of the ST and its geometric parameters. For a real "thick" torus of an arbitrarily smaller radius, the equation for the Lagrange ring takes the form of an integral relation, which includes the expression for the torus potential .

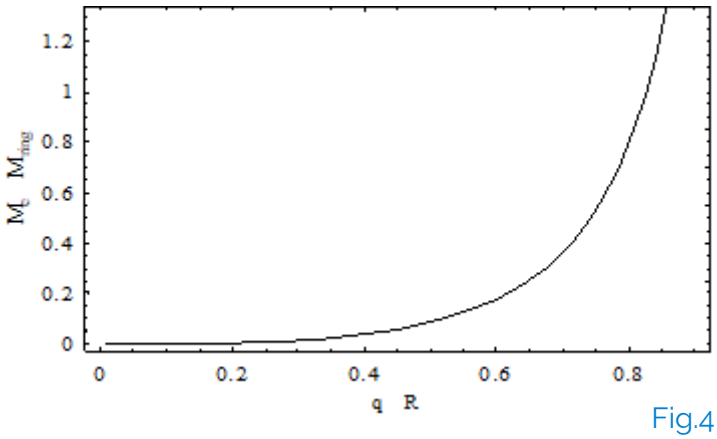

Fig.4

Fig.4. Dependence of the SMBH and the ST mass ratio on the relative position of the Lagrange ring q/R [33,34]

If we use a convenient representation of the potential of a circular torus as a set of thin rings, it will take the form

$$\Phi(\xi,\eta) = G\int_{-a}^{+a} d\eta' \int_{-\sqrt{R^2-a^2}}^{+\sqrt{R^2-a^2}} d\xi' \cdot \rho \cdot \phi(\xi,\eta;\xi',\eta') \quad , \tag{5.2}$$

where $\xi - \eta$ are Cartesian coordinates x-z, counted from the center of the torus cross-section x-z, $\phi(\xi,\eta;\xi',\eta')$ is the potential created at a point ξ ,η by a thin ring ξ',η' of unit density (see, for example, [37-39]).

For a homogeneous torus with constant density

$$\Phi = \frac{M_{ring}}{2\pi^2 R a^2}\tilde{\Phi} \quad , \tag{5.3}$$

where $\tilde{\Phi}(x,z)$ is the specific torus potential per density unit.

The external and internal potentials of the torus were estimated in [39] using these relations. They can be used in numerical-analytical calculations of the effect of ST on the SMBH mass, determined by the reverberation method (Bacal, detailed theory developed by R.Blandford and McKee) [34-36] by the measured delay $c\tau$, which appears in the virial relation of the type (the region of instability is assumed for simplicity to lie in the plane z=0)

$$(\Delta V)^2 = \frac{GM_c}{c\tau} + \frac{M_{ring}}{2\pi^2 R a^2}\tilde{\Phi}(x - c\tau, z) \quad . \tag{5.4}$$

London Journal of Research in Science: Natural and Formal

Let us illustrate this with a simplified example, when we replace the actual (from the point of view of the influence of gravity) part of the torus by a cylinder of the same (small) radius *a*, located at a distance of a large torus radius *R* from the AGN center. In the model we will assume that the position of the Lagrange ring coincides with the inner boundary of the torus, i.e. has coordinate *(R-a)*. Then the force of attraction to the cylinder at its boundary is equal to $2\pi Ga\rho$. Equating its force of attraction to the black hole, we obtain

$$\frac{GM_c}{(R-a)^2} = 2\pi G \cdot \frac{M_{ring}}{2\pi^2 Ra}.$$

Or in our model example

$$\frac{(R-a)^2}{2\pi Ra} = \frac{M_c}{M_{ring}}, \tag{5.5}$$

whence follows

$$\frac{a}{R} = 1 + \pi\frac{M_c}{M_{ring}} - \sqrt{\left(1+\pi\frac{M_c}{M_{ring}}\right)^2 - 1}. \tag{5.6}$$

With a large mass of black holes ($\varepsilon = \pi M_c / M_{ring} >> 1$) $a/R \approx M_{ring}/2\pi M_c$; otherwise a massive obscuring torus ($\varepsilon << 1$) $a/R \approx 1-\sqrt{2\varepsilon} = 1-\sqrt{2\pi M_c / M_{ring}}$.

Thus, the position of LRs and, accordingly, the region of broad lines $c\tau$ in the reverberation method, which coincides with the region of instability near the LR (up to the distance to the stable orbits closest to the LR), is affected by a correction determined by the ratio of the masses of the ST and SMBH. Returning to the torus potential and using the virial theorem, as is done in the cited papers, we can estimate it more accurately.

Note, that the dynamical model of a clumpy torus in the gravitational field of a supermassive black hole (based on ALMA observations of the velocity field of the obscuring torus NGC1068 [42]) without taking into account the pressure of radiation of accretion disk is discussed by Bannikova, et al, in [43] in the frame of N-body simulations.

APPENDIX A. PARTICLE-TO-TORUS ATTRACTION [23]

Using the simple reasoning may show that a test particle near the inner side of a self-gravitating torus is subjected to the force attracting it to a torus. First, let us consider a thin torus which extreme case is a cylinder. In fact, the test particle will be attracted to the cylinder. This alone means that the test particle inside a torus is subjected to the force directed to this latter, or to put it more precisely – to the torus part nearest to the particle.

Let us represent a torus as a system of concentric rings. Consider the elementary case, i.e. attraction of a test particle to diametrically opposite ring areas. Select two “sectors”, with their vertices at the test particle and with a small angular span, symmetric with respect to diameter of the ring passing through the test particle. Let us consider the forces of particle attraction to the opposite arcs of a ring inside sectors. If a particle is at the center of the ring, they balance each other (Fig.Aa). When decentering the

particle (along the chosen diameter), we may see that the arc mass increases (or decreases) linearly with distance from the particle, while the force changes inversely as square of distance (Fig.Ab). Therefore, the attraction force from a "distant" arc decreases, though the arc length increases, while the force of attraction to the nearest arc increases, though the arc length decreases with the particle approaching it.

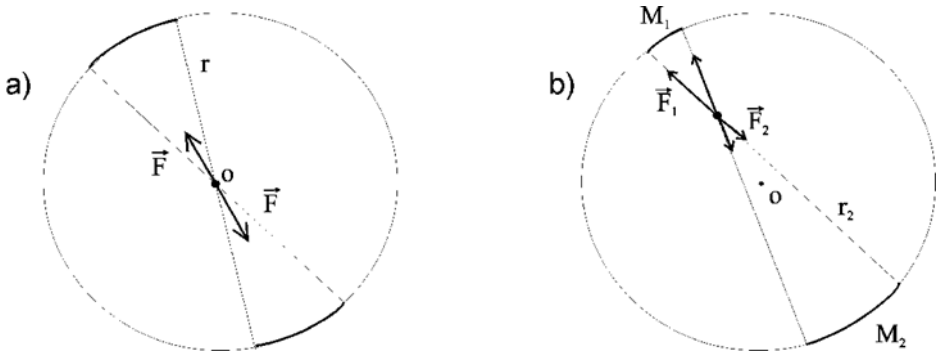

Fig. A1. Scheme of a test particle-to-ring attraction. Fragment of Fig. from the work of the BBK [23]. In the collection "Nonlinear Waves 2004"

An uncompensated force of particle-to-ring attraction and, accordingly, that of particle-to-torus appear. Expanding the span angle we are compelled to proceed from elementary formulas to integrals, though this does not change anyhow the fact of the matter and the result. It will be noted that in the case of a sphere (with the similar reasoning) the mass attracting a particle is proportional to the area on a sphere cut by a solid angle. Therefore, decentering the particle saves the exact compensation of forces: the mass is changed quadratic with the distance and is compensated by inverse dependence of the force vs. square distance. Therefore, as is notorious, a test particle inside a sphere (as against a torus) is subjected to no gravitational force.

The previous reasoning is sustained by the calculation of trajectories of test particles (Fig.A2a). Examples of trajectories for the "vertical" symmetry plane motion are shown in FigA2 [23, 44]. As can be seen from Fig.A2a and Fig. A2b, at small energies, the particle travels around a circle with minor radius, coiling around a ring (Fig.A2a shows the particle's planar motion, Fig.A2b shows the presence of orbital motion). Such motions correspond to a thin vortex (the first stage of evolution possible). With larger particle energy, different complicated trajectories appear (see, e.g. [45]).

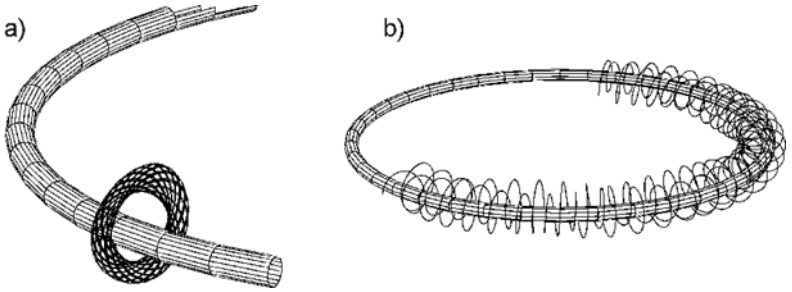

ACKNOWLEDGEMENTS

The paper was reported by Zoom in the department of theoretical physics of the Kharkiv National University seminar (chairs of E.Eserskaja and A.Zvyagin). My deep gratitude also to Voronel's and Laptev's families (especially to Vanya Laptev) for kind support from their side, Editorial of LJRS and Irina Kholodna fund for financial support, to my colleague and friend S.A. Poslavskyi for useful discussions and to Elena Bannikova for inspirationally participation in the work [14]

REFERENCE

1. Peterson BM. An Introduction to Active Galactic Nuclei,CUP: Cambridge 1997, Online ISBN: 9781139170901, 2012.
2. Netzer H. The Physics and Evolution of Active Galactic Nuclei, Cambridge, UK: CUP, 2013. AnnRevAstAp, 2015, 53: 365.
3. Antonucci R. Unified models for active galactic nuclei and quasars. ARA&A, 1993, 31: 473
4. Netzer H. Revisiting the Unified Model AGN. Annu. Rev. Astron. Astrophys. 2015, 53: 365-408.
5. Britzen S. Black Holes in a Violent Universe. New Astronomy Reviews, 2012, 56: 33–36.
6. Popovic LC. Supermassive binary black holes and emission lines in active galactic nuclei. New Astronomy Reviews, 2012, 56: 74.
7. De Rosa A et al. The quest for dual and binary supermassive black holes: A multi-messenger view. New Astronomy Reviews, 2019, 86: 101525
8. Liu BF. and Erlin Qiao. Accretion around black holes: The geometry and spectra, iScience, 2022, 25: 103544.
9. Salpeter EE. Accretion of interstellar matter by massive objects. ApJ, 1964, 140: 796–800.
10. Beskin VS. MHD Flows in Compact Astrophysical Objects: Accretion, Winds and Jets. 2009.
11. Blandford R, Meier D and Readhead A. Relativistic Jets from Active Galactic Nuclei. ARA&A, 2019, 57:467.
12. Romero GE. The content of astrophysical jets. Astronomical note, 2021, 342 (5): 727.
13. Faucher-Giguere C-A and Quataert E. The physics of galactic winds driven by active galactic nuclei. MNRAS, 2012, 425: 605–622.
14. Bannikova EYu and Kontorovich VM. A Dipole Vortex Model of Obscuring Tori in Active Galaxy Nuclei. Astronomy Reports, 2007, 51: 264.
15. Brightman M. et al,· Breaking the limit: Super-Eddington accretion onto black holes and neutron stars, Astro 2020 White Paper, 2019; arXiv:1903.06844.
16. Babadzhanyants MK. and Belokon ET. Optical manifestations of the superluminal expansion of the components of the millisecond radio structure of the 3C 345 quasar. Astrophysics, 1985, 23: 459.
17. Komberg BV. (1992). Quasars and Active Galactic Nuclei. In Kardashev NS. (ed.). Astrophysics on the Threshold of the 21st Century, 1992: 253.
18. Voloshchuk VM. Kinetic theory of coagulation, Leningrad: Gidrometeoizdat, 1984. 284 p.
19. Kontorovich VM, Kats AV and Krivitsky DS. “Explosive" evolution of galaxies in a model of coalescence events and an epoch of quasar formation. Pis'ma Zh. Eksp. Teor. Fiz. 1992, 55(1): 3-7.
20. Kontorovich VM. The evolution of galaxies in the mirror of the coagulation equation. LTP, 2016, 43: 41.
21. Born M. and Wolf E. Principles of Optics, CUP, 2013.
22. Landsberg GS, Optics. Moscow: Fizmatlit, 2003. 848 p.
23. Bannikova EYu Bliokh KYu and Kontorovich VM. Evolution and collapse of self-gravitating toroidal vortex. In: Nonlinear Waves’ 2004, Nizhniy Novgorod, 2004, 14p.
24. Bliokh KYu and Kontorovich VM. On the Evolution and Gravitational Collapse of a Toroidal Vortex. Journal of Experimental and Theoretical Physics, 2003, 96(6) : 985–992.
25. Lamb H. Hydrodynamics (Dover Books on Physics) Cambridge University Press, 1947.
26. Milne-Thomson L. Theoretical Hydrodynamics, Ed. Journal of Applied Mechanics 1968.
27. Larichev VD and Reznik GM. On two-dimensional solitary Rossby waves. Soviet Doklady, 1967, 231: 1077.
28. Kats AV and Kontorovich VM. Merger Driven Explosive Evolution of Distant Galaxies (Minor Mergers). Astrophysical Bulletin, 2013, 68: 273; astro-ph/1309.0957, 2013.
29. Mateos S, et al. Survival of the Obscuring Torus in the Most Powerful AGN. The ApJLetters, 2017, 841:L18.

30. Landau LD and Lifshitz EM. Hydrodynamics. Nauka, Moscow (1986).
31. Kontorovich VM and Poslavskyi SA. Swirling self-gravitating vortex as the imagination of the Hoag's ring galaxy, LTP, 2022, 48(5): 413-419.
32. Bannikova EYu and Kontorovich VM. Invited talk: Central mass influence on evolution of self-gravitating toroidal vortex. In: International Symposium Topical Problem of Nonlinear Wave Physics, St. Petersburg- – N.Novgorod, 2005.
33. Bannikova Elena Yu. The structure and stability of orbits in Hoag-like ring systems. MNRAS, 2018, 476: 3269–3277.
34. Gaskell M. What broad emission lines tell us about how active galactic nuclei work. New Astronomy Reviews, 2009, 53: 140.
35. Blandford RD and McKee CF. Reverberation mapping of the emission line regions of Seyfert galaxies and quasars, Astrophysical Journal, 1982, 255: 419.
36. Cackett EM, Bentz MC and Kara E. Reverberation mapping of active galactic nuclei: From X-ray corona to dusty torus, iScience, 2021, 24: 102557 .
37. Kondratyev BP. Potential Theory. New methods and problems with solutions. Moscow, Mir, 2007.
38. Batygin BB and Toptygin IN. Contemporary electrodynamics, Part 1. Moscow-Izhevsk: "R & C dynamics", 2003, 736 p. (in Russian).
39. Bannikova EYu, Vakulik VG and Shulga VM. Gravitational potential of a homogeneous circular torus: a new approach, MNRAS, 2011, 411: 557.
40. Peterson BM. The Broad-Line Region in Active Galactic Nuclei. Lect. Notes Phys. 2006, 693: 77–100.
41. Marziani P and Sulentic JW. Estimating black hole masses in quasars using broad optical and UV emission lines. New Astronomy Reviews, 2012, 56:49.
42. Garcia-Burillo S, Combes SF, Ramos Almeida C, et al. ALMA images the many faces of the NGC 1068 torus. A&A, 2019, 61: 632.
43. Bannikova E, Sergeyev A, Akerman N, Berczik P, Ishchenko M, Capaccioli M and Akhmetov V. Velocity and velocity dispersion maps for interpretation of ALMA observations. Mon. Not. R. Astron. Soc., 2021,503, Issue 1: 1459-1472.
44. Bliokh KYu and Kontorovich VM. JETP, 2003, 123: 1123 (astro-ph/0407320); 2003, Letters to Astron.J., 29, 816 (astro-ph/0409067).
45. Lavrentyev MA and Shabat BV. Problems of Hydrodynamics and their Mathematical Models. 1973, Nauka, Moscow. 416 pp. (in Russian).

This page is intentionally left blank

Role of Time Delay on Sensitivity and Hopf-Bifurcation between two Competing Plant Populations under Allelopathy

Dipesh & Pankaj Kumar

Lovely Professional University

ABSTRACT

The study of dynamical interactions between two competing plant populations under the influence of allelochemicals is a current area of active research. In this paper, we have studied the effect of allelochemicals on the plant populations of two competing species model with particular emphasis on time reliant variations in their densities. Positivity, Boundedness, Equilibrium point is calculated. We have also studied the stability of the dynamics system about non-zero equilibrium points with the help of the Routh-Hurwitz theorem. The system shows asymptotic stability when the value of delay parameter is less than the critical value. Hopf-bifurcation occurs when the value of the delay parameter is greater than the critical value. In addition, we calculate the sensitivity analysis of the dynamics system to understand how the various sources of uncertainty in a model contributes to the overall uncertainty.

Keywords: allelopathy, sensitivity analysis, delay, hopf-bifurcation.

Classification: DDC Code: 581.5247 LCC Code: QK911

Language: English

London Journals Press

LJP Copyright ID: 925691
Print ISSN: 2631-8490
Online ISSN: 2631-8504

London Journal of Research in Science: Natural and Formal

Volume 22 | Issue 10 | Compilation 1.0

Role of Time Delay on Sensitivity and Hopf-Bifurcation between two Competing Plant Populations under Allelopathy

Dipesh[α] & Pankaj Kumar

ABSTRACT

The study of dynamical interactions between two competing plant populations under the influence of allelochemicals is a current area of active research. In this paper, we have studied the effect of allelochemicals on the plant populations of two competing species model with particular emphasis on time reliant variations in their densities. Positivity, Boundedness, Equilibrium point is calculated. We have also studied the stability of the dynamics system about non-zero equilibrium points with the help of the Routh-Hurwitz theorem. The system shows asymptotic stability when the value of delay parameter is less than the critical value. Hopf-bifurcation occurs when the value of the delay parameter is greater than the critical value. In addition, we calculate the sensitivity analysis of the dynamics system to understand how the various sources of uncertainty in a model contributes to the overall uncertainty.

Keywords: allelopathy, sensitivity analysis, delay, hopf-bifurcation.

Author: Department of Mathematics, Lovely Professional University, Phagwara-144411, Punjab, India.

I. INTRODUCTION

Allelopathic interference mechanisms are extremely difficult, if not impossible, to distinguish from interference due to competing in economic and environmental conditions. Plant interference is defined as any physical or chemical process that causes a plant's development to be radiated over time as a result of the availability of another plant. Rihan and Bocharov investigate the descriptive and analytical relevance of delay in plant populations, metabolism, and other areas, as well as the sensitivity analysis in numerical modeling utilizing the delay differential equation, applying a direct method [1]. Rihan also examined the sensitivity analysis for dynamic systems with delays utilizing the direct technique when the model's parameters are not constant but change over time [2]. Kalra and kumar studies the role of delay in plant development under the effect of toxic metal [3]. Dipesh and Kumar worked on stimulatory and inhibitory allelopathy effects on two competing plant populations [4]. Gupta et al. studied the effect of allelopathic on competing harvesting species and observed that realizes allelochemicals are inhibitory for each other [5]. In a predator-prey model with discrete delays, a systematic analysis was presented for several types of stabilities such as absolute stability, conditionally stability, and bifurcation [6]. The nature of exponential characteristic equation zeros studied in depth was proposed by Wei and Ruan [7]. A Lotka-Volterra competitive system for two planktonic ecosystems in the presence of toxicity proposed by Chattopadhyay [8]. Monica et al. observed that allelopathy may also be considered a significant impact in nature crops when coping with cooperative or sequential development of a variety of plants [9]. The response of aquatic competitive models in the handling of toxic substances is a hot topic right now. The impact of toxic chemicals on the formation of algal communities is explored utilizing a variety of dynamics factors, including stability, elimination of both species, and delay differential equation systems. [10-14]. The impact of toxic effects on phytoplankton populations is being studied by aquatic ecological specialists [15-16]. Sun et al. suggested a response–

London Journal of Research in Science: Natural and Formal

diffusion equation to show the interaction between plant transcriptional protections and herbivore transcriptional protections. They assumed that the plant harmed by the herbivore using transcriptional protections requires some response time, which may be expressed by time delay [17]. Kumar and Dipesh studied the effect of allelochemicals on competing plant populations using time lag [18].

In light of the above discussion, a mathematical method is developed for analyzing the role of delay in the allelopathic effect competition of a community of plants when one population releases allelochemicals and affects the other, while the other organism does not develop any allelochemicals and discovers that the affecting population may be pushed to death.

II. MATHEMATICAL MODEL

A set of nonlinear ordinary differential equations lead the classic two-species Lotka-Volterra type competition model.

$$\frac{dP_1}{dt} = P_1\left(c_1 - \alpha_1 P_1 - \beta_{12} P_2\right) \tag{1}$$

$$\frac{dP_2}{dt} = P_2\left(c_2 - \alpha_2 P_2 - \beta_{21} P_1\right) \tag{2}$$

Where $P_1$and P_2 are the two competing plant populations species respectively, c_1 and $c_2$are the cell proliferation rate of 1st and 2nd plant populations respectively, α_1 and α_2 are the intraspecific competition of 1st and 2nd plant population species. β_{12} and β_{21} are the interspecific competition of 1st and 2nd plant population species. The units of c_1, c_2, α_1 and α_2 is the number of days per cell and days is the unit of time.

We take an additional term into the Lotka-Volterra equation of second plant population species to the model for the allelochemicals interaction.

$$\frac{dP_1}{dt} = P_1\left(c_1 - \alpha_1 P_1 - \beta_{12} P_2\right) \tag{3}$$

$$\frac{dP_2}{dt} = P_2\left(c_2 - \alpha_2 P_2 - \beta_{21} P_1 + \gamma P_1 P_2\right) \tag{4}$$

γ denotes the role of allelochemicals substance realized by second plant population species and affects the first plant population with having all parameters have same biotic explanation above. Release of allelochemicals is not suddenly and but some discrete time delay is required for plant population to mature. This time delay is introduced in the release of allelochemicals by 1st plant population and introduces discrete delay into the intraspecific competition term of both plant populations. The competition model is defined for the system as:

$$\frac{dP_1}{dt} = P_1\left(c_1 - \alpha_1 P_1(t-\tau) - \beta_{12} P_2\right) \tag{5}$$

$$\frac{dP_2}{dt} = P_2\left(c_2 - \alpha_2 P_2(t-\tau) - \beta_{21} P_1 + \gamma P_1(t-\tau) P_2\right) \tag{6}$$

Where $P_1 \geq 0,\ P_2 \geq 0\ for\ all\ t\ \&\ P_1(t-\tau)\ \&\ P_2(t-\tau) = Constant\ for\ t \in [0, \tau]$.

For understanding a biological phenomena we check the basis properties like positivity, boundedness, equilibrium and stability. These properties would make it easier to calculate the validity of the biological phenomena. Whereas delay occurs in nature and takes part in the system to understand the dynamics of biological phenomena.

2.1 Boundedness of Solution

Let $W = P_1 + P_2$

$$\frac{dW}{dt} = \frac{dP_1}{dt} + \frac{dP_2}{dt}$$

$$\text{Let } \chi = \left(\alpha_1, \alpha_2, \beta_{12}, \beta_{21}, \gamma\right) \& P_1(t-\tau) \cong P_1, P_2(t-\tau) \cong P_2$$

$$\frac{dW(t)}{dt} \leq \chi\left(P_1 + P_2\right) - (c_1 + c_2)$$

$$\Rightarrow 0 \leq \chi W - (c_1 + c_2)$$

$$\Rightarrow 0 \leq W \leq \frac{(c_1+c_2)}{\chi}$$

All solution of $(3) - (4)$ lying in the region $S = \left[\left(P_1, P_2\right) \in R_+^2 : 0 \leq W \leq \frac{(c_1+c_2)}{\chi}\right] as\ t \to \infty\ \forall$ positively initial value $P_1 \geq 0,\ P_2 \geq 0\ \forall t\ \&\ P_1(t-\tau), P_2(t-\tau) = constant\ for\ t \in [0,\tau] \in S \subset R_+^2$.

2.2 Positivity of Solution

All the given solution of $(5) - (6)$ are positive with initial condition $P_1 \geq 0,\ P_2 \geq 0\ \forall t\ \&\ P_1(t-\tau), P_2(t-\tau) = constant\ for\ t \in [0,\tau]$. The significance of $\left(P_1, P_2\right)$ remain positive for all $t > 0$.

From Equ. (5)

$$\frac{dP_1}{dt} \geq \left(c_1 - \alpha_1 P_1 - \beta_{12} P_2\right) P_1$$

$$\Rightarrow \frac{dP_1}{P_1} \geq \left(c_1 - \frac{(c_1+c_2)}{\chi}(\alpha_1 - \beta_{12})\right) dt$$

$$\Rightarrow P_1 \geq e^{-\left(c_1 - \frac{(c_1+c_2)}{\chi}(\alpha_1 - \beta_{12})\right)t}$$

Similarly we calculate $P_2,\ \forall P_1 \geq 0,\ P_2 \geq 0$.

2.3 Equilibrium Points for the Solution

Several equilibrium point for the dynamical system (5)-(6) are $E_{00},\ E_{10}, E_{01}, E^*$ exist with no limitation on the variable of the dynamical system

$$E_{00}: (0,0)\ \ (zero\ equilibrium\ point)$$

London Journal of Research in Science: Natural and Formal

$$E_{10}: \left(\frac{c_1}{\alpha_1}, 0\right) \qquad (axial\ equilibrium\ point,\ unstable)$$

$$E_{01}: \left(0, \frac{c_2}{\alpha_2}\right) \qquad (axial\ equilibrium\ point,\ unstable)$$

$$E^*\left(P_1^*, P_2^*\right) \qquad (Non-zero\ equilibrium\ point,\ stable)$$

We study only non-zero equilibrium point $E^*\left(P_1^*, P_2^*\right)$

From Equ. (5)

$$\frac{dP_1^*}{dt} = P_1^*\left(c_1 - \alpha_1 P_1^* - \beta_{12} P_2^*\right)$$

$$P_1^* \neq 0,\ so\ c_1 - \alpha_1 P_1^* - \beta_{12} P_2^* = 0$$

$$\text{We get } P_1^* = \frac{c_1 - \beta_{12} P_2^*}{\alpha_1} \tag{7}$$

and similarly we calculate $P_2^* = \frac{c_1}{\alpha_2 - \beta_{21} - \gamma P_1^*}$

Put the value of P_2^* in (7) we get a quadratic equation in P_1^*

$$\alpha_1 \gamma P_1^{*2} - \left(\gamma c_1 + \alpha_1\alpha_2 + \alpha_1\beta_{21}\right)P_1^* + c_1\alpha_2 + c_1\beta_{21} - \beta_{12}c_1 = 0$$

Which have two roots

$$P_{1,2}^* = \frac{\left(\gamma c_1 + \alpha_1\alpha_2 + \alpha_1\beta_{21}\right) \pm \sqrt{\left(\gamma c_1 + \alpha_1\alpha_2 + \alpha_1\beta_{21}\right)^2 - 4\alpha_1\gamma(c_1\alpha_2 + c_1\beta_{21} - \beta_{12}c_1)}}{2\alpha_1\gamma} \tag{8}$$

Local Stability of Equilibrium Point $\left(P_1^*, P_2^*\right)$ and Hopf-Bifurcation

$$\frac{dP_1^*}{dt} = P_1^*\left(c_1 - \alpha_1 P_1^*(t-\tau) - \beta_{12} P_2^*\right)$$

$$\frac{dP_2^*}{dt} = P_2^*\left(c_2 - \alpha_2 P_2^*(t-\tau) - \beta_{12} P_2^* + \gamma P_1^*(t-\tau) P_2^*\right)$$

The characteristic equation of the system is

$$A(\lambda, \tau) = \lambda^2 + \left(a_1 e^{-\lambda\tau} + a_2\right)\lambda + b_1 + e^{-\lambda\tau} d = 0 \tag{9}$$

Where $a_1 = 2\gamma P_2^* - 2\alpha_2 P_2^* - 2\alpha_1 P_1^*$

$$a_2 = 3\beta_{12} P_2^* - c_1 - c_2$$

$$b_1 = c_1c_2 - 2\beta_{12}P^*_2c_1$$

$$d = c_1 + c_2 + c_3 + c_4$$

Where $c_1 = 2P^*_2\left(c_1\alpha_2 - \beta_{12}\alpha_2 P^*_2\right)$, $c_2 = 2\alpha_1P^*_1\left(c_2 - 2\beta_{12}P^*_2 - 2\right)$, $c_3 = -2\alpha_2P^*_2$

$$c_4 = \gamma P^*_2(2c_1 + 2\beta_{12}P^*_2 - 2 + \beta_{12}P^*_1)$$

Clearly $a_1, a_2, b_1, and\ d$ all are positive.

If we put $\tau = 0$ in Equ. (9), we get

$$\lambda^2 + \left(a_1 + a_2\right)\lambda + b_1 + d = 0 \tag{10}$$

With the help of Routh-Hurwitz criteria, root of Equ. (10) will be negative real part, i.e., the dynamical system is stable iff:

$$\left(g_1\right): \left(a_1 + a_2\right) > 0,\ \left(g_2\right): \left(b_1 + d\right) > 0\ Which\ is\ true.$$

At $\tau = 0$, E^* is locally asymptotically stable when $\frac{\alpha_1}{\beta_{12}} > max\left[\frac{\beta_{21}}{\alpha_2}, \frac{P^*_1}{P^*_2}\right]$

E^* will be locally asymptotically stable for $\tau \geq 0$ when the real part of $A(\lambda, \tau)$ is -ve and $A(i\omega, \tau) \neq 0$ for every real ω *and* $\tau \geq 0$. Now we calculate the negative real component of the root moves for the positive real component root when the value of τ is different.

Assume $\lambda = i\phi,\ \phi > 0$ be the root of Equ. (9), then (9) became

$$(i\phi)^2 + \left(a_1e^{-i\phi\tau} + a_2\right)(i\phi) + b_1 + e^{-i\phi\tau}d = 0$$

$$\Rightarrow -\phi^2 + \left(a_1(cos\phi\tau - isin\phi\tau) + a_2\right)(i\phi) + b_1 + d(cos\phi\tau - isin\phi\tau) = 0$$

Separate real and imaginary part, we get

$$\phi^2 - b_1 = a_1\phi sin\phi\tau + dcos\phi\tau \tag{11}$$

$$a_2\phi = dsin\phi\tau - a_1\phi cos\phi\tau \tag{1 2}$$

Squaring and adding (11) and (12), we get

$$\phi^4 + \left(a_2^2 - 2b_1 - a_1^2\right)\phi^2 + b_1^2 - d^2 = 0 \tag{13}$$

Equ. (13) have two roots

$$\phi^2_{1,2} = \frac{\left(a_1^2 + 2b_1 - a_2^2\right) \pm \sqrt{\left(a_2^2 - 2b_1 - a_1^2\right)^2 - 4(b_1^2 - d^2)}}{2} \tag{14}$$

No roots of $\phi_{1,2}^2$ is +ve if:

$$(g_3): \left(a_1^2 + 2b_1 - a_2^2\right) < 0 \; and \; \left(b_1^2 - d^2\right) > 0 \; or \; \left(a_2^2 - 2b_1 - a_1^2\right)^2 < 4(b_1^2 - d^2)$$

So, Equ. (14) doesn't have positive root if condition (g_3) hold.

Lemma 1. Root of Equ. (9) have negative real part for all $\tau \geq 0$, if $(g_1) - (g_2)$ hold.

Other side if

$$(g_4): \left(b_1^2 - d^2\right) < 0 \; or \; \left(a_1^2 + 2b_1 - a_2^2\right) > 0 \; and \; \left(a_2^2 - 2b_1 - a_1^2\right)^2 = 4(b_1^2 - d^2)$$

W shows that Equ. (11) have one positive root, which is ϕ_1^2. If

(g_5): $\left(b_1^2 - d^2\right) > 0 \; or \; \left(a_1^2 + 2b_1 - a_2^2\right) > 0 \; and \; \left(a_2^2 - 2b_1 - a_1^2\right)^2 > 4(b_1^2 - d^2)$ Which shows that Equ. (11) have two positive roots, which is $\phi_{1,2}^2$.

In $(g_4) \; and \; (g_5)$, when we change the value of τ, root of Equ. (9) are purely imaginary. With the help of Equ. (11)-(12) critical value of $\tau_i^{\pm}$ of τ are calculated :

$$\tau_i^{\pm} = \frac{1}{\phi_{1,2}} cos^{-1} \frac{(\phi_{1,2}^2 - b_1)}{d} + \frac{2i\pi}{\phi_{1,2}}, \; i = 0, 1, 2, \ldots \tag{15}$$

The above discussion can be condensed in succeeding by S. Raun [5].

Lemma 2. (i) Equ. (9) has a pair of imaginary roots $\pm i\phi_1$, if $(g_1) - (g_2) \; and \; (g_4)$ hold and $\tau = \tau_i^+$.

(ii) Equ. (9) has a pair of imaginary roots $\pm i\phi_2 (\pm i\phi_1)$ respectively, if $(g_1) - (g_2) \; and \; (g_5)$ hold and $\tau = \tau_i^- (\tau = \tau_i^+ \; resp.)$.

Our exception is the negative real part shifted toward positive real part when $\tau > \tau_i^+$ & $\tau < \tau_i^+$. We check the possibilities

$$\tau_i^{\pm} = \mu_i^{\pm}(\tau) + i\phi_i^{\pm}(\tau); i = 0, 1, 2, 3 \ldots.$$

The roots of Equ. (9) satisfied. $\mu_i^{\pm}(\tau_i^{\pm}) = 0, \; \phi_i^{\pm}(\tau_i^{\pm}) = \phi_{1,2}$

We can verify that the following transversely conditions

$$\frac{d}{d\tau}\left(Re\lambda_i^+(\tau_i^+)\right) > 0 \; and \; \frac{d}{d\tau}\left(Re\lambda_i^-(\tau_i^-)\right) < 0$$

It shows that $\tau_i^{\pm}$ varies with different values. The distribution of the Equ. (9) zeros are determined by the S. Raun,

Theorem 1. Let $\tau_i^+ (l = 0, 1, 2, 3...)$ be defined by Equ. (15).

(1) If $(g_1), (g_2)$ hold, then all of root (9) have -ve real part $\forall \tau \geq 0$.

(2) If $(g_1), (g_2)$ *and* (g_4) hold and when $\tau \epsilon [0, \tau_0^+)$, then all of root (9) have negative real parts. When $\tau = \tau_0^+$, then (9) has a pair of purely imaginary roots $\pm i\phi_1$. When $\tau > \tau_0^+$, (9) has at least one $+ ve$ real part root.

(3) If $(g_1), (g_2)$ *and* (g_5) carry & +ve integer n s.t. $0 < \tau_0^+ < \tau_0^- < \tau_1^+ < \tau_1^+ ..... < \tau_{n-1}^- < \tau_n^+$ and there is n oscillation from stable to unstable. Which shows $\tau \epsilon [0, \tau_0^+)$, $(\tau_0^-, \tau_1^+) ..... (\tau_{n-1}^+, \tau_n^+)$ all the roots of Equ. (9) have $- ve$ real parts. When $\tau \epsilon [0, \tau_0^+)$, $(\tau_0^-, \tau_1^+) ..... (\tau_{n-1}^+, \tau_{n-1}^-)$ & $\tau > \tau_n^+$, Equ. (9) has at least one root with real parts.

Sensitivity Analysis of State variables w.r.t. model parameter

The model contains constant parameters in this article. The 'Direct Method' is used for estimating the coefficients of generalized sensitivity. The direct approach is based on assuming all parameters as fixed then somehow, by utilizing the sensitivity equations with initial solution of equations, the sensitivity coefficients are calculated. When all the parameters $\alpha_1, \alpha_2, \beta_{12}, \beta_{21}, \gamma$ in the proposed system (5) - (6) are assumed to be constant, then sensitivity analysis may simply involve finding the solution's partial derivatives with regard to each parameter in this case. As an example, if parameter c_1 considered then partial derivatives of the solution $(P_1, P_2,)$ w.r.t. c_1 gives rise to following set of sensitivity equation:

$$\frac{dS_1}{dt} = S_1 P_1 - \beta_{12}(S_2 P_1 - S_1 P_2) - 2\alpha_1 P_1(t - \tau) S_1(t - \tau) \quad (16)$$

$$\frac{dS_2}{dt} = S_2 P_2 - 2\left(\alpha_2 P_2(t - \tau) S_2(t - \tau) - \gamma P_1(t - \tau) S_2\right)\beta_{21}\left(S_1 P_2 + S_2 P_1\right) + \gamma S_1(t - \tau) P_2^2 \quad (17)$$

Where $S_1 = \frac{\partial P_1}{\partial c_1}$, $S_2 = \frac{\partial P_2}{\partial c_2}$,

This sensitivity equation system (16) - (17) is then solved together with the original equation system (5)-(6) to approximate the sensitivity of the variable $(P_1, P_2,)$ to the parameter c_1. The system variables' sensitivity to the function, and the related approach and statement apply.

Sensitivity of Variable to Parameter C_1

In Figure1, the variable consumption coefficient c_1 causes no difference and adjustment in the quality of the state vector allelochemical P_1 and P_2 which remain stable and tends to zero, as we decrease the value of $c_1 = 1.8$ *to* $c_1 = 2.6$. It indicates that the state will be less sensitive variable P_1 and P_2 to the variable c_1. However, in the case of the equal rang of value of c_1, the state variable amount of allelochemicals P_2 goes for the considerable change as shown by $\alpha_1, \alpha_2, \beta_{12}, \beta_{21}, \gamma$. It indicates that when the delayed value of the coefficient decreases, the rate of allelochemicals increases. It also remains stable.

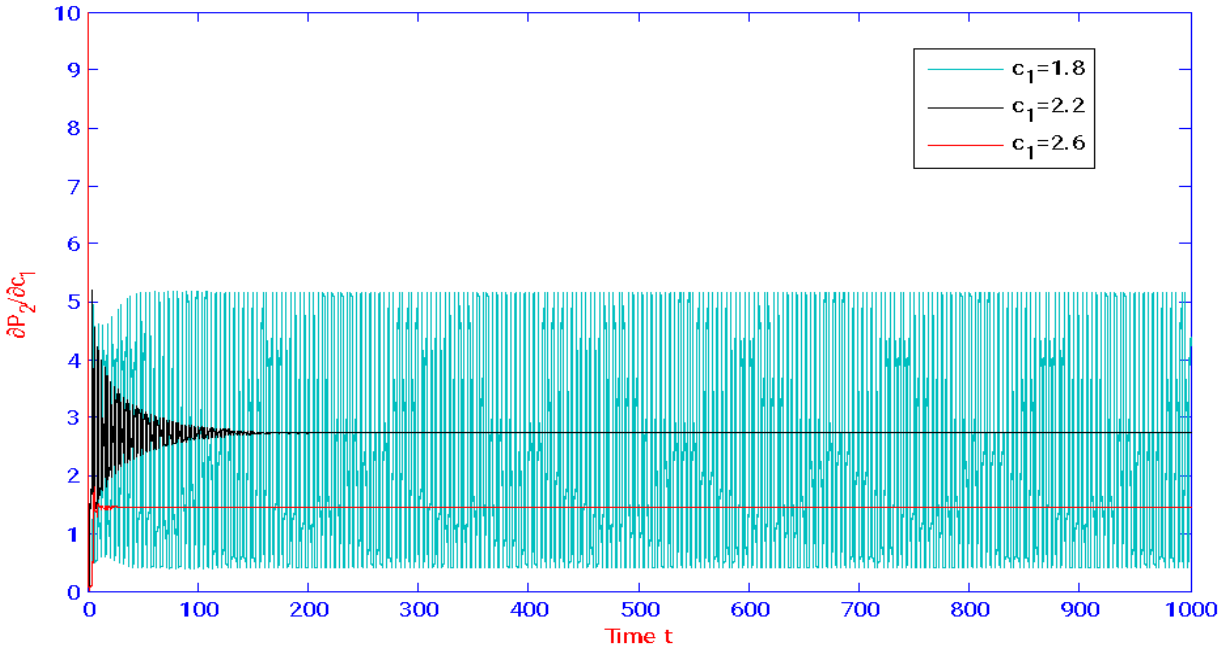

Figure 1: Time series graph between partial changes in allelochemicals P_1 for different value of coefficientc_1.

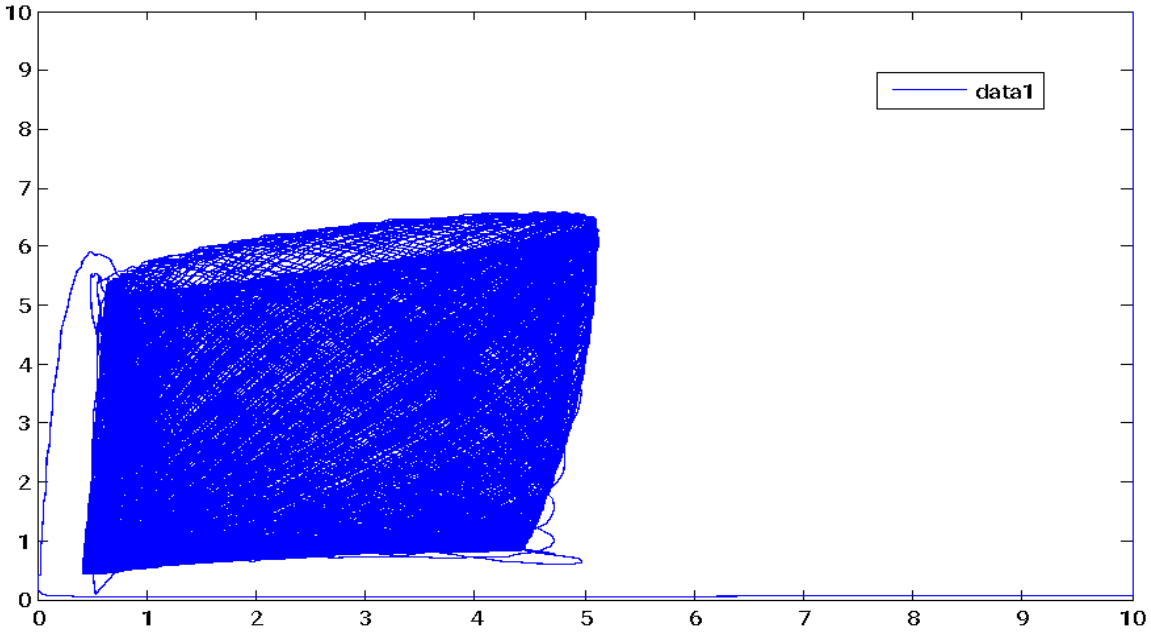

Figure 2: Phase diagram of plant populations P_1, P_2 when the value of $c_1 = 1.8$.

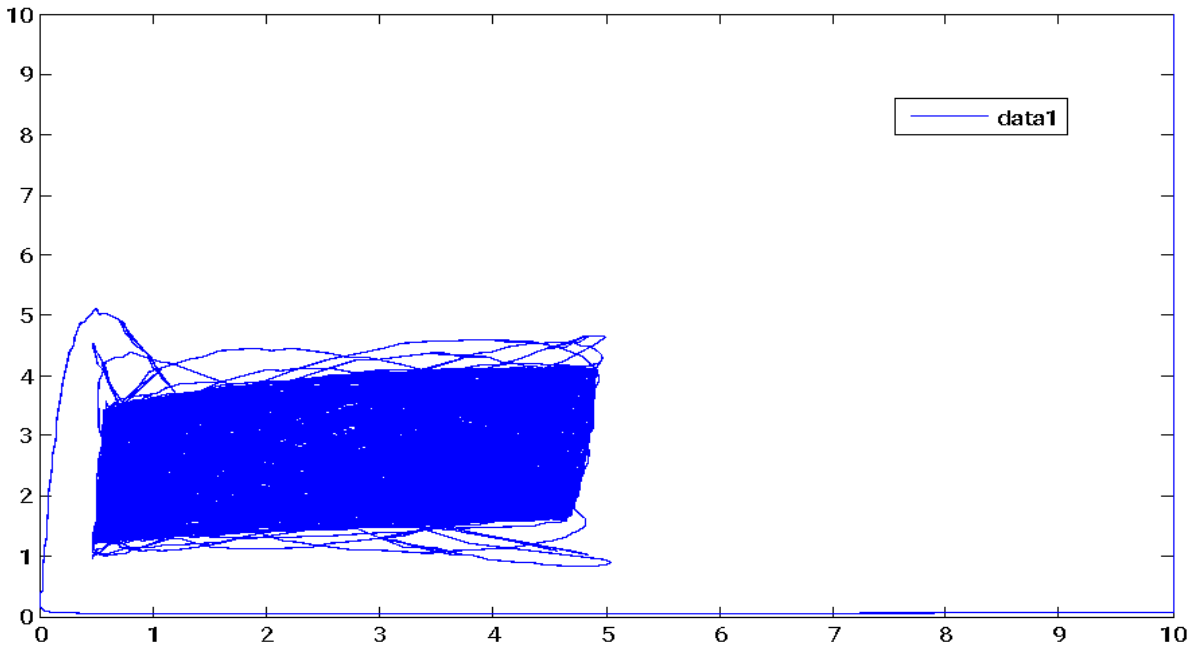

Figure 3: Phase diagram of plant populations P_1, P_2 when the value of $c_1 = 2.2$.

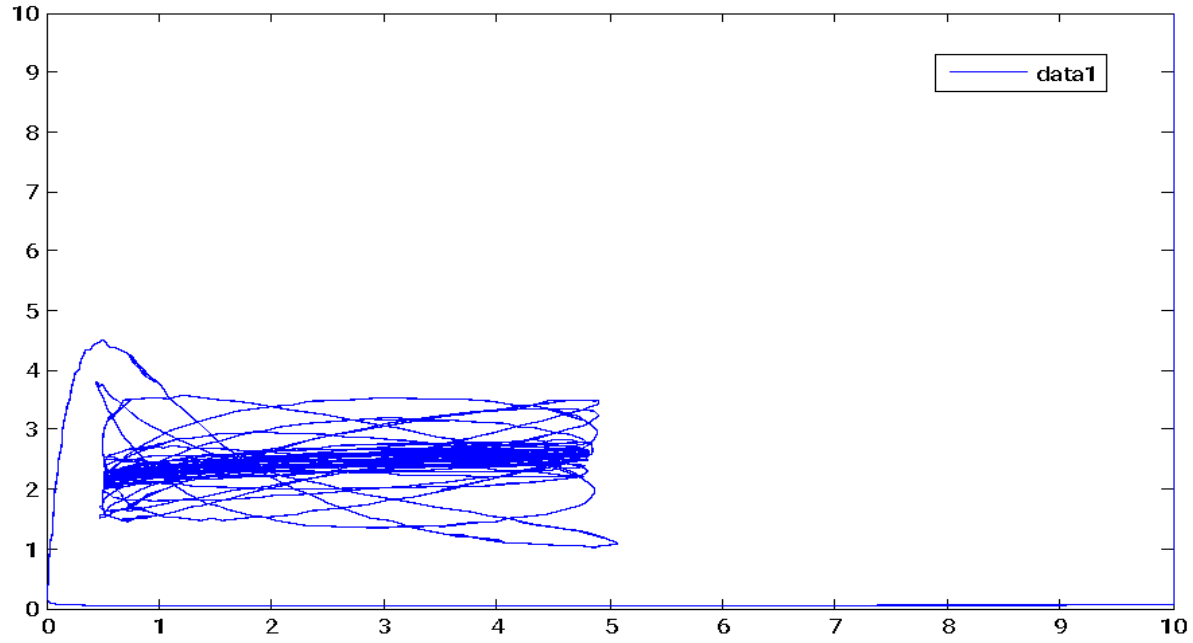

Figure 4: Phase diagram of plant populations P_1, P_2 when the value of $c_1 = 2.6$.

Numerical Example

The calculation is conducted with MATLAB to coordinate the analytical result with the aid of a numerical. The behavior of the system is demonstrated for the given sets of values:

$$c_1 = 1.8,\ c_2 = 2,\ \alpha_1 = 0.8,\ \alpha_2 = 0.7,\ \beta_{12} = 0.015,\ \beta_{21} = 0.05,\ \gamma = 0.008$$

The dynamical system (5)-(6) changes the behavior around the equilibrium, varying with delay parameter value.

III. RESULT AND DISCUSSION

Figure1 represent the sensitivity of dynamical system with respect to the parameter c_1. Which shows that the stability of the system oscillate with different value of $c_1 = 1.8\ to\ 2.6$, putting other parameters are constant. Kalra and Kumar studied the effect of toxic metal on sensitivity analysis of the dynamical system with parametric value $\beta = 0.3\ to\ 0.7$, $\gamma = 0.05\ to\ 0.2\ and\ \alpha = 0.5\ to\ 0.9$, and worked on the role of delay on two plant population with parametric value $k_N = 1$, $k_{NM} = 0.3$, $\alpha = 0.9$, $I = 0.5$, $\gamma = 0.2$, $\delta_1 = 0.2, \delta_2 = 0.8, \delta_3 = 0.4$, found that in the absence of delay system is stable ($\tau = 0$) and at $\tau < 1.373$ system shows the asymptotically stable but when the value $\tau \geq 1.373$, system shows the Hopf-Bifurcation (3). Rihan's also conduct an experimental studied in point of subinterval $[0, 2\tau]$ on sensitivity analysis and observed that when change the value of τ in interval $[0, \tau]$ the system shows the change. Also observed that τ play a significant role in the field of sensitivity analysis (2).

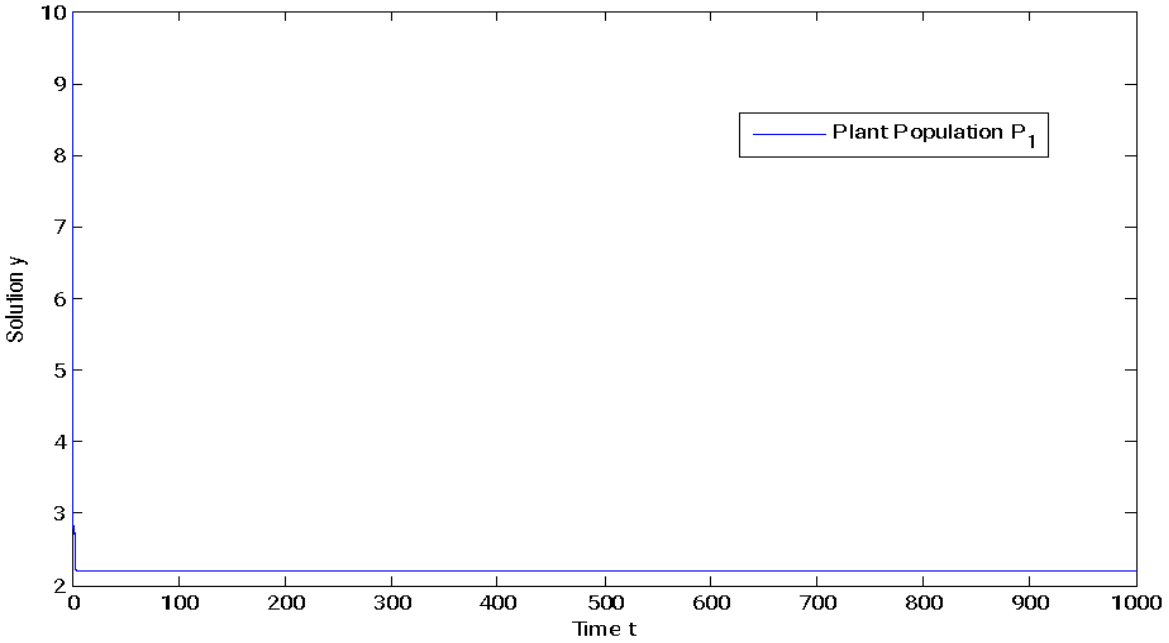

Figure 5: At $\tau = 0$, the plant population P_1 is stable.

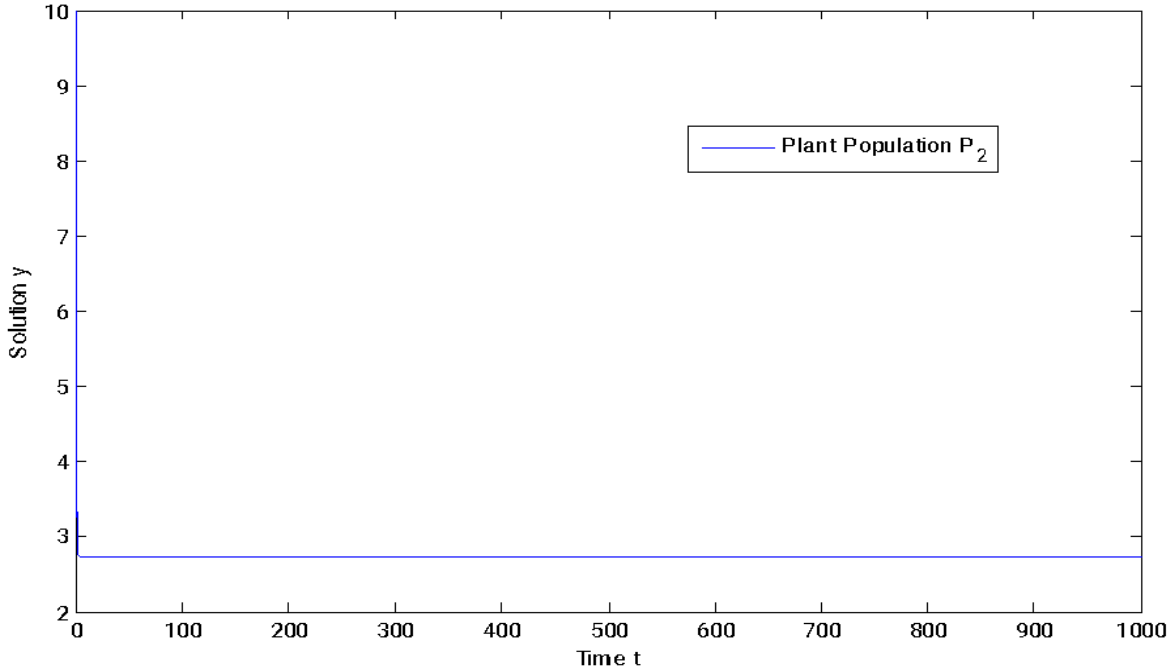

Figure 6: At $\tau = 0$, the plant population P_2 is stable.

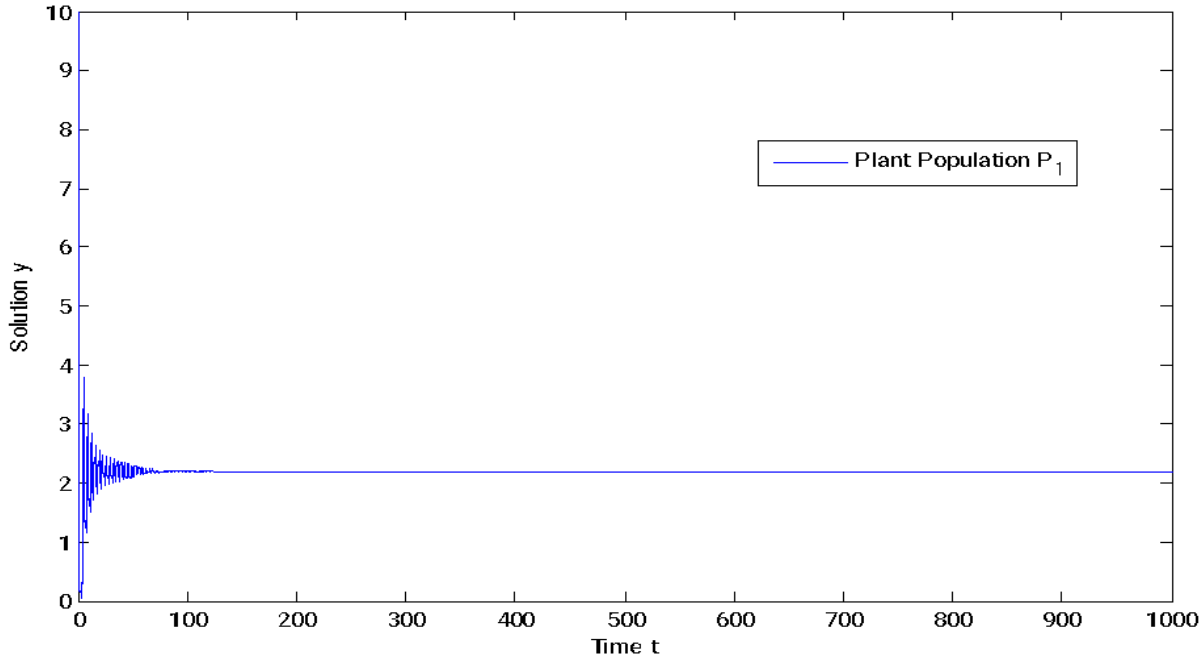

Figure 7: At $\tau < 0.8129$, the plant population P_1 loses its stability and shows the asymptotically stable.

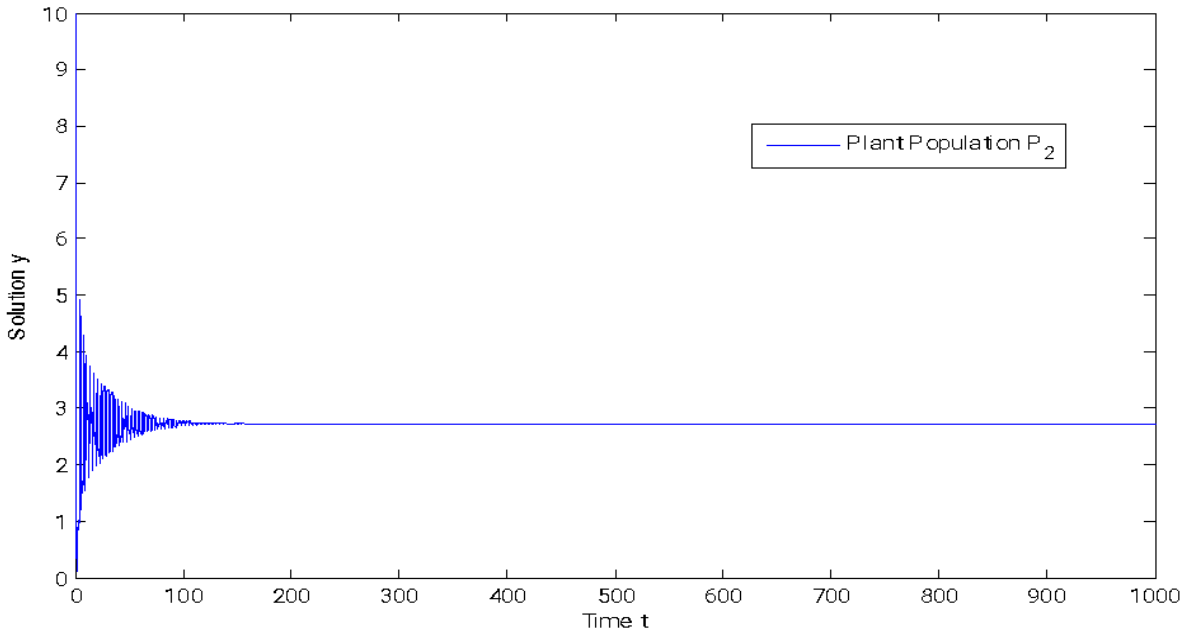

Figure 8: At $\tau < 0.8129$, the plant population P_2 loses its stability and shows the asymptotically stable.

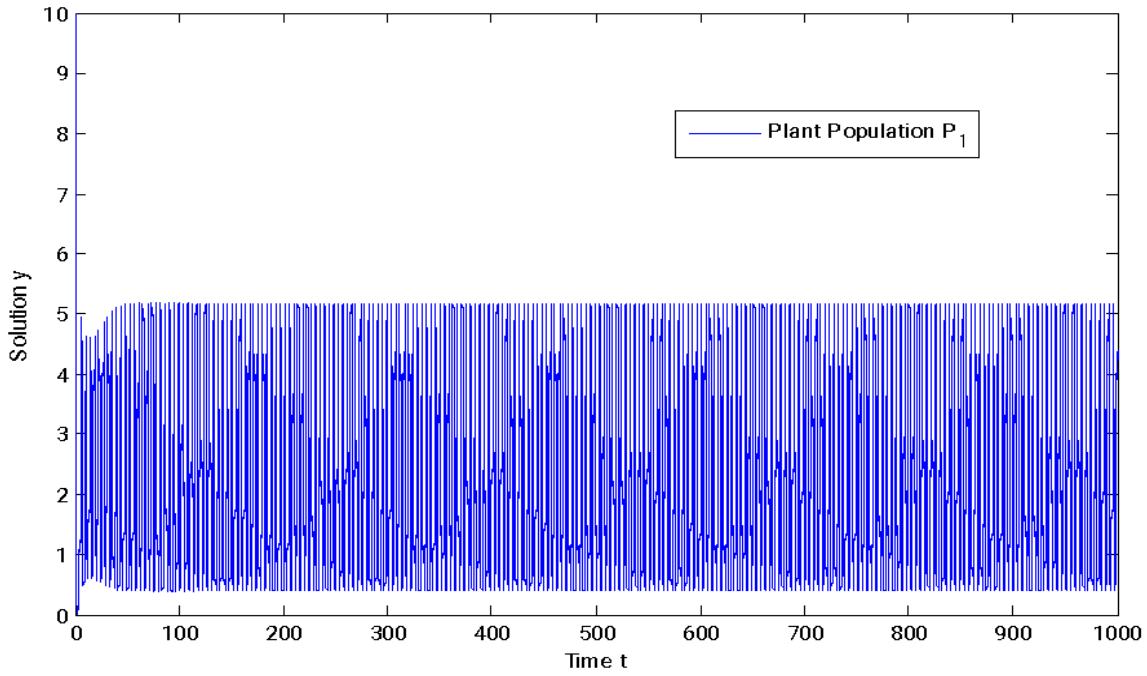

Figure 9: At $\tau \geq 0.9999$, the plant population P_1 loses its asymptotically stability and shows hopf-bifurcation.

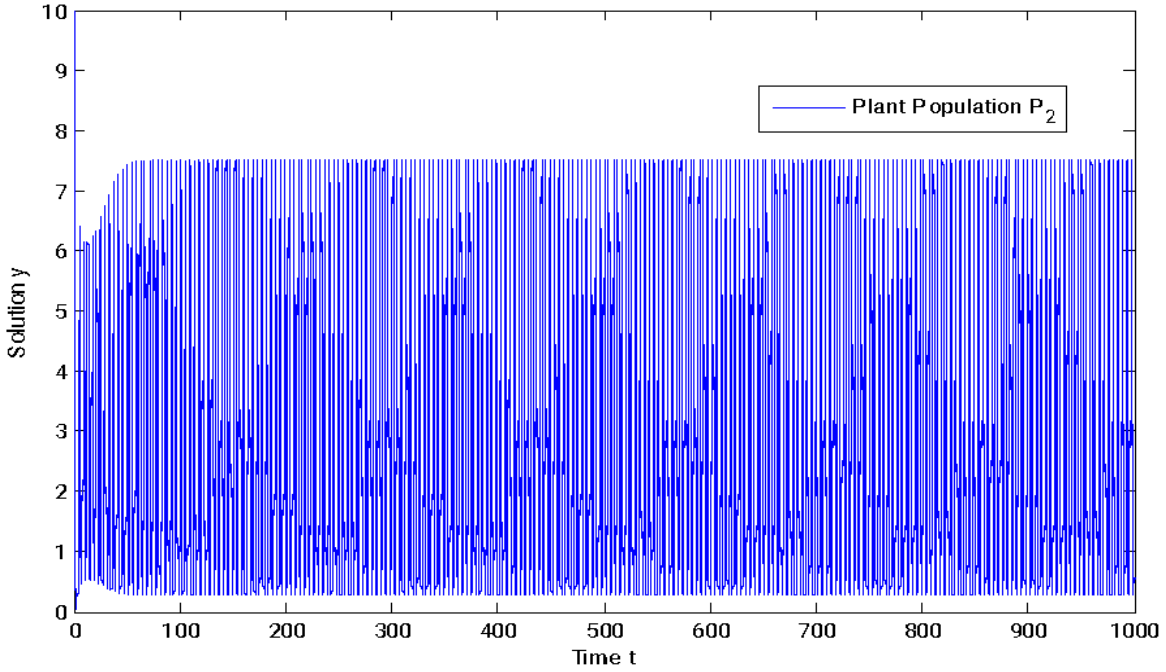

Figure 10: At $\tau \geq 0.9999$, the plant population P_2 loses its asymptotically stability and shows hopf-bifurcation.

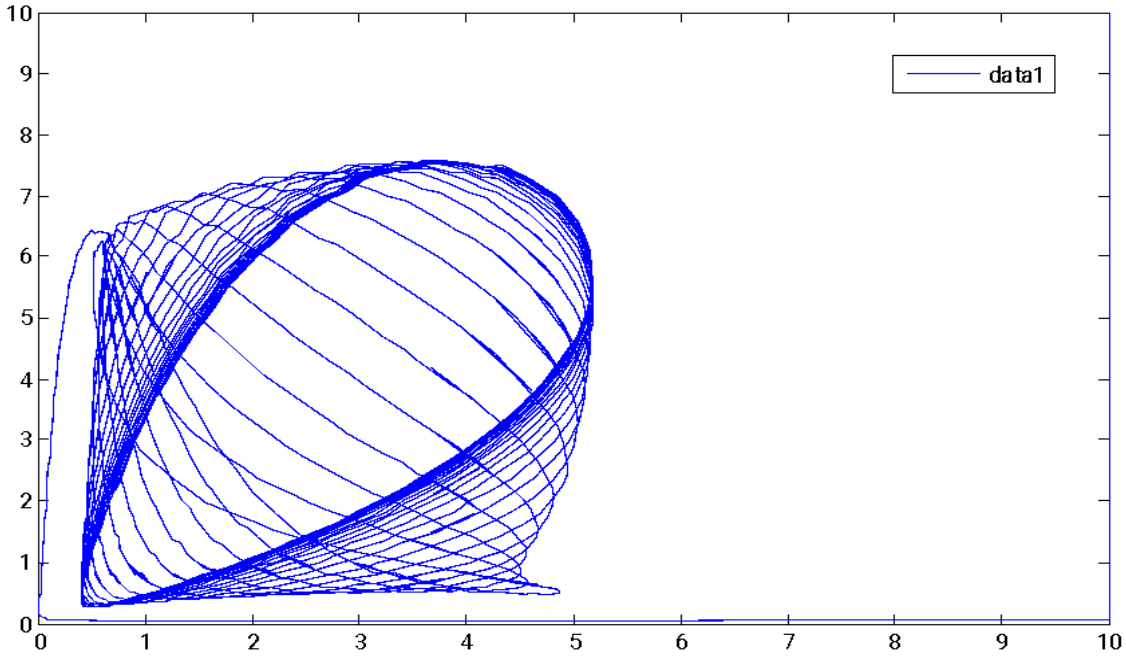

Figure 11: Phase diagram of the plant populations $\tau \geq 0.9999$.

IV. CONCLUSION

In this paper, we have studied the effect of allelochemicals on sensitivity and stability analysis of two competing plant populations. We have used the "Direct Method" to study the sensitivity analysis of the dynamics system. Further we have checked how the different parameters (cell proliferation, intraspecific and interspecific competition) affects the stability of the model. We have calculated the

sensitivity analysis for c_1 parameter by varying its value from $c_1 = 1.8\ to\ 2.2\ to\ 2.6$. It has been observed that at $c_1 = 2.6$, stability in a dynamic system occurs. Further we have calculated the stability of the dynamic system about non-zero equilibrium point. It has been examined that when there is no delay, the system shows stability. And when the value of the delay parameter is less than the critical value, the system loses its stability and shows asymptotically stability. The equilibrium point loses its asymptotically stability when the value of the delay parameter is greater than the critical value and starts showing the Hopf-bifurcation. In MATLAB we use the dde23 command for graphical representations.

Declarations

Ethical Approval

The declaration is “not applicable”.

Competing Interests

The declaration is “not applicable”.

Author’s Contributions

Dipesh- Conceptualization, Formal analysis, Investigation, Methodology and Software

Pankaj Kumar- Supervision

Funding

The declaration is “not applicable”.

Availability of data and materials

The declaration is “not applicable”.

REFERENCES

1. Bocharov, Gennadii A., and Fathalla A. Rihan. "Numerical modelling in biosciences using delay differential equations." *Journal of Computational and Applied Mathematics* 125, no. 1-2 (2000): 183-199.
2. Rihan, Fathalla A. "Sensitivity analysis for dynamic systems with time-lags." *Journal of Computational and Applied Mathematics* 151, no. 2 (2003): 445-462.
3. Kalra, P., and P. Kumar. "The Study of Time Lag on Plant Growth under the Effect of Toxic Metal: A Mathematical Model." *Pertanika Journal of Science & Technology* 26, no. 3 (2018).
4. Dipesh and Pankaj Kumar. "Modelling the stimulatory and inhibitory allelopathic effects on competing plant populations." In *AIP Conference Proceedings*, vol. 2435, no. 1, p. 020044. AIP Publishing LLC, 2022.
5. Gupta, R. P., Malay Banerjee, and Peeyush Chandra. "The dynamics of two-species allelopathic competition with optimal harvesting." *Journal of Biological Dynamics* 6, no. 2 (2012): 674-694.
6. Ruan, Shigui. "Absolute stability, conditional stability and bifurcation in Kolmogorov-type predator-prey systems with discrete delays." *Quarterly of applied mathematics* 59, no. 1 (2001): 159-173.
7. Ruan, Shigui, and Junjie Wei. "On the zeros of transcendental functions with applications to stability of delay differential equations with two delays." *Dynamics of Continuous Discrete and Impulsive Systems Series A* 10 (2003): 863-874.

8. Chattopadhyay, J. "Effect of toxic substances on a two-species competitive system." *Ecological Modelling* 84, no. 1-3 (1996): 287-289.
9. Scognamiglio, Monica, Brigida D'Abrosca, Assunta Esposito, Severina Pacifico, Pietro Monaco, and Antonio Fiorentino. "Plant growth inhibitors: allelopathic role or phytotoxic effects? Focus on Mediterranean biomes." *Phytochemistry Reviews* 12, no. 4 (2013): 803-830.
10. Chen, Fengde, Zhong Li, Xiaoxing Chen, and Jitka Laitochová. "Dynamic behaviors of a delay differential equation model of plankton allelopathy." *Journal of Computational and Applied Mathematics* 206, no. 2 (2007): 733-754.
11. Li, Zhong, and Fengde Chen. "Extinction in two dimensional non autonomous Lotka–Volterra systems with the effect of toxic substances." *Applied Mathematics and Computation* 182, no. 1 (2006): 684-690.
12. Li, Zhong, and Fengde Chen. "Extinction in periodic competitive stage-structured Lotka–Volterra model with the effects of toxic substances." *Journal of computational and applied mathematics* 231, no. 1 (2009): 143-153.
13. Liu, Zhijun, Jianhua Wu, Yiping Chen, and Mainul Haque. "Impulsive perturbations in a periodic delay differential equation model of plankton allelopathy." *Nonlinear Analysis: Real World Applications* 11, no. 1 (2010): 432-445.
14. Fergola, P., E. Beretta, and M. Cerasuolo. "Some new results on an allelopathic competition model with quorum sensing and delayed toxicant production." *Nonlinear Analysis: Real World Applications* 7, no. 5 (2006): 1081-1095.
15. Rice, E. L. "Allelopathy, 2nd edn Academic Press." *New York, USA* (1984).
16. Samanta, G. P. "A two-species competitive system under the influence of toxic substances." *Applied Mathematics and Computation* 216, no. 1 (2010): 291-299.
17. Sun, Gui-Quan, Su-Lan Wang, Qian Ren, Zhen Jin, and Yong-Ping Wu. "Effects of time delay and space on herbivore dynamics: linking inducible defenses of plants to herbivore outbreak." *Scientific Reports* 5, no. 1 (2015): 1-10.
18. Kumar, P., and Dipesh. Effect of time delay on dynamic of plant competition under allelopathy. *Mathematical Methods in the Applied Sciences*.

This page is intentionally left blank

God Does Not Play Dice

Elie W'ishe Sorongane

University of Kinshasa, Kinshasa

ABSTRACT

Historically, science and religion have diverged on the question of the origin of all that exists. The theory of evolution in history demonstrates by proven experimental facts that the development of the universe took several billion years while the theory of creation in the Bible is content to affirm that God created all that exists in just six days. Great was our surprise when we realized that in fact these two theories did not contradict each other but on the contrary, they agreed almost perfectly. The sequence of events in both theories is the same; but it is only the time scales used that differ. We can then associate the two theories thanks to the relationship of time dilation drawn from special relativity. This ends up highlighting the acceleration of the expansion of the universe. We then showed that this accelerated expansion was simply the result of a Meissner effect between the superconducting dark matter and the magnetic fields of the stars. We also demonstrate the relativistic effect of this acceleration on the flow of time on earth. The new description of the expansion of the universe presented in this work then allowed us to question the theory of the big bang and the hypothesis of an unlimited or endless expansion of the universe.

Keywords: theory of evolution, theory of creation, time dilation, expansion of the universe, dark matter, dark energy.

Classification: DDC Code: 306.6094109034 LCC Code: BL41

Language: English

London Journals Press

LJP Copyright ID: 925644
Print ISSN: 2631-8490
Online ISSN: 2631-8504

London Journal of Research in Science: Natural and Formal

Volume 22 | Issue 10 | Compilation 1.0

God Does Not Play Dice

Elie W'ishe Sorongane

SUMMARY

Historically, science and religion have diverged on the question of the origin of all that exists. The theory of evolution in history demonstrates by proven experimental facts that the development of the universe took several billion years while the theory of creation in the Bible is content to affirm that God created all that exists in just six days. Great was our surprise when we realized that in fact these two theories did not contradict each other but on the contrary, they agreed almost perfectly. The sequence of events in both theories is the same; but it is only the time scales used that differ. We can then associate the two theories thanks to the relationship of time dilation drawn from special relativity. This ends up highlighting the acceleration of the expansion of the universe. We then showed that this accelerated expansion was simply the result of a Meissner effect between the superconducting dark matter and the magnetic fields of the stars. We also demonstrate the relativistic effect of this acceleration on the flow of time on earth. The new description of the expansion of the universe presented in this work then allowed us to question the theory of the big bang and the hypothesis of an unlimited or endless expansion of the universe.

Keywords: theory of evolution, theory of creation, time dilation, expansion of the universe, dark matter, dark energy.

Author: Physics Department, University of Kinshasa, Kinshasa, Democratic Republic of the Congo.

I. INTRODUCTION

Religion and science have always differed on a question which is no longer the most important and the most difficult of all the questions that man has ever had to ask himself during his life on earth, I quote: what is the origin of the universe? Or in more colloquial language, where does all that exists come from?

Seeking the answer to this question, scientists, relying on archaeological excavations and using sophisticated dating technologies, presented a theory of evolution in which they demonstrated that the universe grew over several billion years to get to the state it is in today.

The Christian relies on his faith in God to believe what is written in the first chapter of the Bible's book of Genesis. The religion, in its theory of creation, then asserts that God created all that exists in just six days.

By studying in depth the two theories cited above, you cannot imagine our surprise when we discovered that in reality, there was no point of contention between the said theories. The sequence of events in both theories is the same; but it is only the time scales used that differ. We will then use the relation of time dilation drawn from special relativity to associate the two theories. This will allow us to highlight the acceleration of the expansion of the universe. We will then show that this accelerated expansion of the universe is simply the result of a Meissner effect between the superconducting dark matter and the magnetic fields of stars. Finally, we will also demonstrate the relativistic effect of the accelerating expansion of the universe on the flow of time on earth.

These texts are the result of long scientific research on the question of the origin of the universe, regardless of the nature of the source. You will therefore be led here to adopt a purely scientific meaning and to call “theory” what most of our contemporaries would qualify as “mythical” or even “mystical”.

Let us first begin by briefly recalling the essence of the two fundamental theories on the origin of the universe.

II. REVIEW OF THE TWO FUNDAMENTAL THEORIES ON THE ORIGIN OF THE UNIVERSE

2.1. Theory of creation

The Bible tells the story of God creating the world in six days (Genesis 1) [4]. We can summarize this story with the following few lines:

- 1st day :
  - Creation of the heavens and the earth.
  - Creation of light.
- 2nd day:
  - Creation of an expanse between the waters above and the waters below.
  - Creation of the expanse called sky.
- 3rd day:
  - Creation of a distinction between a single "dry" land mass and a single "sea" water mass.
  - Creation of vegetation.
- 4th day:
  - Creation of stars.
  - Creation of the sun and the moon.
- 5th day:
  - Creation of marine animals.
  - Creation of birds.
- 6th day:
  - Creation of land animals (mammals, reptiles, etc.)
  - Creation of man.

2.2 Theory of Evolution

Archeology and biology allow us to go back several billion years in the past and date the appearance of life on earth. The different dating techniques used today have allowed us to draw a prehistoric timeline that can be summarized as follows [5]:

- -15 billion years: Birth of the Universe
- -4.6 billion years ago: Birth of the earth
- -600 million years: Gondwana (cluster of unique earth) and cluster of water.
- -430 million years ago: Appearance of vegetation
- -350 million years ago: Appearance of life in the sea
- -220 million years ago: Appearance of large reptiles and dinosaurs
- -150 million years ago: Appearance of birds
- -3 million years ago: Appearance of man (Australopithecus Lucy).

NB:

By considering the order in which events occur in each of the two theories, we see that there is a certain consistency. The sequence of events in both theories is virtually the same. The way life was created by God in the theory of creation and the way life appeared on earth in the theory of evolution are exactly the same with one very small exception: the appearance of birds. Today there are some theories that claim that the ancestors of birds cohabited on earth with the dinosaurs. We therefore ask archaeologists and historians to carry out more thorough excavations on the flying species which will most probably allow us to make some correction to the theory of evolution and then to realize a perfect match with the theory of creation.

III. TIME DILATION

Since Albert Einstein and his theory of special relativity, we now know that time is relative. Time is no longer an absolute physical magnitude as was certain in classical physics, but rather a parameter which can vary from one observer to another. This variation of time is relative to the state of motion of one observer relative to another; the time therefore depends on the observer.

In the relativistic theory, Einstein considers an inertia observer who measures the duration or the proper time τ of a well-determined event. Another observer who moves at a speed v relative to the first, will measure for the same event, the duration or the time t given by:

$$t = \gamma \tau \qquad (1)$$

Where γ is the Lorentz constant, given by:

$\gamma = \frac{1}{\sqrt{1-\frac{v^2}{c^2}}}$; with c, the speed of light in vacuum $(c = 3.10^8 \frac{m}{s})$.

Equation (1) is called “the time dilation relationship” [2].

Let's go back to our two fundamental theories on the origin of the universe. In the theory of creation, God measures the same proper time $\tau = 24h = 86400\ s$ for six distinct events. Man (a terrestrial observer), in the theory of evolution, measures time $t_n (n = 1, 2, 3, 4, 5, 6)$ for the same events. Thanks to the relationship of time dilation $t_n = \gamma\tau$, we will deduce the different speeds v_n of movement of an earthly observer with respect to God in the biblical theory of creation. And moreover, this same Bible clearly alludes to the dilation of time in the second book of Peter, I quote: "but there is one thing, beloved, that you must not ignore, which is that, before Lord, a day is like a thousand years, and a thousand years are like a day” (2 Peter 3:8).

For the first, the second, and the fourth day of creation, we have no information in the theory of evolution that allows us to calculate $t_1, t_2\ et\ t_4$. On the other hand, for the third, the fifth and the sixth day, we have:

- Third day: According to the theory of creation, this event starts from Gondwana until the appearance of vegetation. The theory of evolution gives:

$$t_3 = -\ 430.10^6 - \left(-\ 600.10^6\right) = 17.10^7\ years = 536\,112.10^{10} s$$

we have:

$$t_n = \gamma\tau$$

$$\Leftrightarrow v_n = \sqrt{1 - \frac{\tau^2}{t_n^2}}\, c \qquad (2)$$

$$\Leftrightarrow v_n = \Gamma_n . c$$

With:

$$\Gamma_n = \sqrt{1 - \frac{\tau^2}{t_n^{\ 2}}} \qquad (3)$$

Let's calculate Γ_3, we have:

$$\Gamma_3 = \sqrt{1 - \frac{\tau^2}{t_3^{\ 2}}}$$

$$\Longrightarrow \Gamma_3 = 0,999999999999999999987$$

- Fifth day: According to the theory of creation, this event starts from the appearance of life in the sea until the appearance of birds. The theory of evolution gives:

$$t_5 = -\ 150.10^6 - \left(-\ 350.10^6\right) = 2.10^8\ years = 63072.10^{11} s$$

Let's calculate Γ_5, we have:

$$\Gamma_5 = \sqrt{1 - \frac{\tau^2}{t_5^2}}$$

$\Rightarrow \Gamma_5 = 0,99999999999999999990$

– Sixth day: According to the theory of creation, this event starts from the appearance of land animals (mammals, reptiles, etc.) until the appearance of man. The theory of evolution gives:

$$t_6 = -3.10^6 - \left(-210.10^6\right) = 207.10^6\ years = 6\,527\,952.10^9 s.$$

Let's calculate Γ_6, we have:

$$\Gamma_6 = \sqrt{1 - \frac{\tau^2}{t_6^2}}$$

$\Rightarrow \Gamma_6 = 0,999999999999999999999991$

Remarks :

a) We notice that the velocities $v_n = \Gamma_n c$ are very close to the speed of light. This does not mean that at that time the earth was moving at a speed v_n, very close to the speed of light, with respect to a fixed point in space. Rather, it means that she was moving at a relative speed v_n with respect to God. God not being matter but spirit, the fundamental law of special relativity on the limit speed (the speed of light is the limit speed that a material body in motion can reach) could not be applied to him. He could therefore move at any speed, even at speeds greater than the speed of light. It is therefore a question here of two beings, of completely different natures, moving in space: God, who is spirit, moves at a speed $v \approx c$ and man, who is of material nature, moves with the earth at a speed $v \ll c$ (see Figure 1).

b) We also notice that $\Gamma_3 < \Gamma_5 < \Gamma_6$. Hence, by generalizing, we can write: $\Gamma_1 < \Gamma_2 < \Gamma_3 < \Gamma_4 < \Gamma_5 < \Gamma_6 ... < \Gamma_n$.

Equation (2) then allows us to write:

$$v_1 < v_2 < v_3 < v_4 < v_5 < v_6 ... < v_n .$$

This can be interpreted as an acceleration of the expansion of the universe which we will describe in the next section.

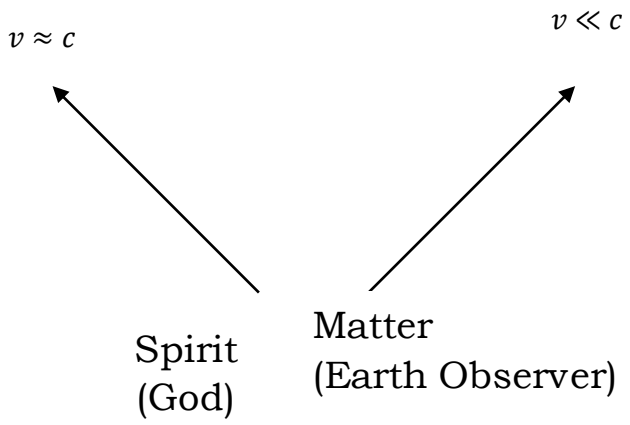

Figure 1: The earth moves at a relative speed v_n with respect to God.

IV. THE EXPANSION OF THE UNIVERSE

4.1b Dark matter and dark energy

I was working on astronomy and cosmology when two concepts immediately caught my attention: dark matter and dark energy.

Indeed, by using Newton's laws of gravity, physicists have been able to demonstrate that the visible matter that we can observe in the universe only constitutes 5% of all the mass contained in the universe. In other words, the universe is made up largely, or 95%, of invisible matter. Physicists called it "dark matter", claiming that it was of an unknown form and therefore non-baryonic. I don't understand why this dark matter would be non-baryonic. When you walk through a furnished room that is completely dark, you can touch the furniture even though you can't see it. And the furniture in this room is not made up of non-baryonic particles either. You cannot see this furniture only because it emits radiation in the infrared range which is invisible to the naked eye. A man equipped with infrared glasses would be able to perceive the light coming from these pieces of furniture and he would therefore be able to see them. Likewise, just because we can't clearly see the dark matter in the universe doesn't mean it has to be non-baryonic. In fact, dark matter is baryonic, it is made up of protons, neutrons and electrons like any other matter in the universe. However, this dark matter does not emit radiation in the visible range to be seen, it rather emits in the microwave range which is invisible to the naked eye. It is the cosmic radiation at 2.7 K in the microwave range observed on earth in all directions. This radiation was first observed by chance in 1965 by two American physicists at the Bell Telephone Laboratories in New Jersey, Arno Penzias and Robert Wilson when they were testing a very sensitive microwave detector. In other words, a man equipped with a sensitive detector in the microwave range would be able to see the dark matter that populates the universe by looking in any direction. Thus, we can say that when we look in any direction in the universe, we always come across dark matter and that is why the sky is black at night. This is a solution to Olbers' paradox that we proposed in the article entitled "Quantum Color Theory", published in the "*Open Journal of Applied Sciences*" [9]. But then, where did this dark matter come from? To answer this question, we first need to explain what dark energy is.

Indeed, the universe is in perpetual expansion. In other words, the stars that populate the universe are moving away from each other. This expansion is accelerated; that is to say that the speed at which two celestial bodies move away, one with respect to the other, increases with the distance which separates them. Edwin Hubble calculated the rate of expansion of the universe H_0 (a speed divided by a distance) called the Hubble constant. H_0 is currently estimated at $71 \pm 4 \frac{Km}{\frac{s}{Mpc}}$, which means that two celestial bodies separated by a distance of 1 Mpc, move away from each other at a speed of 71 Km/s (1 parsec = 3.261 light years) [6]. There must therefore exist in the universe a repulsive energy which opposes gravity to produce this expansion. Physicists have attributed this repulsive energy to the empty space that separates the two stars that are moving away from each other. Hence the name dark energy of the vacuum. But, admit that this is curious. Because if the vacuum really has an energy, why does man persist in using matter as a source of energy? He would simply have to create the vacuum and use the energy of the vacuum created. So you understand how absurd it is to affirm that the vacuum has an energy.

We therefore propose here a more realistic explanation of the existence of this repulsive energy in the universe. In fact, to first answer the previous question, namely where the dark matter that abounds in the universe came from, the dark matter that we observe in all directions in the universe is made up of the ancient stars that are extinguished (dead stars). A star's light and heat are produced by nuclear fusion reactions at the star's core. The stability of the star is then due to the fact that the force of gravity (which tends to contract the star) is counterbalanced by the force of thermal pressure (which tends to expand the star). Thus, the higher the mass of a star, the higher its internal temperature. More fusion

reactions then occur in a star of relatively large mass than in a star of relatively small mass. After using all of its nuclear fusion fuel, the relatively high-mass star dies out while the relatively low-mass star continues to burn fuel through nuclear fusion reactions and to emit visible light. Stars that died out in the past therefore have masses greater than those of stars that are still alive today. This explains the fact that the universe contains more dark matter (95%) than visible matter (5%).

An ordinary star with the same chemical composition as the sun is made up essentially of carbon when it dies out. To understand why and how, we just need to observe the different cycles of nuclear fusion reactions in an ordinary star like the sun. We distinguish a series of cycles, connected to each other, some being catalytic cycles.

- IP cycle I (60%):

$p + p \rightarrow d + e^{+} + \nu_{e} + 0,42\ Mev$ (followed by $e^{+} + e^{-} \rightarrow 2\gamma + 1\ Mev$).

$$p + d \rightarrow 23He + \gamma + 5,5\ Mev$$

$$23He + 23He \rightarrow 24He + p + p + \gamma + 12,9\ Mev$$

- PP II cycle (24%), the helium 3 produced above is used:

$$23He + 24He \rightarrow 47Be + \gamma + 1,6\ Mev$$

$$47Be + e^{-} \rightarrow 37Li + \nu_{e} + 1,1\ Mev$$

$$37Li + p \rightarrow 48Be \rightarrow 224He + 17,4\ Mev$$

(catalyst $24He$)

- PP III cycle (1%) (variant of the previous one):

$$23He + 24He \rightarrow 47Be + \gamma + 1,6\ Mev$$

$$47Be + p \rightarrow 58B + \gamma + 0,1\ Mev$$

$$58B \rightarrow 48Be + e^{+} + \nu_{e} \rightarrow 224He + 18,4\ Mev$$

- Bethe CNO cycle (15%)-catalysis by C, N and O:

$$612C + p \rightarrow 713N + \gamma + 1,95\ Mev$$

$$713N \rightarrow 613C + e^{+} + \nu_{e} + 1,5\ Mev$$

$$613C + p \rightarrow 714N + \gamma + 7,54\ Mev$$

$$714N + p \rightarrow 815O + \gamma + 7,35\ Mev$$

$$815O \rightarrow 715N + e^{+} + \nu_{e} + 1,73\ Mev$$

$$715N + p \rightarrow 612C + 24He + 4,96\ Mev$$

During its lifetime, the star therefore transforms its hydrogen into carbon through successive nuclear fusion reactions. The dead star is therefore, to a good approximation, an enormous solid and cold mass of carbon. Since there is no longer any fusion reaction in the extinct star, the only source of heat for the dead star is the radiation that comes from neighboring stars that are still alive. The equilibrium temperature is reached when the amount of energy received by the dead star is equal to the amount of energy it emits in the form of thermal radiation. If this equilibrium temperature is lower than 15 K, the dead star is then in the superconducting state

because the critical temperature of carbon is 15 K [11]. A large-scale Meissner effect then occurs between the superconducting star and the magnetic fields of neighboring living stars. These stars are then repelled by the superconducting star. Hence the expansion of the universe. Notice then that there is opposition between two forces: gravity which tends to bring the living stars closer to the superconducting star and the magnetic repulsion due to the Meissner effect which tends to move the living stars away from the superconducting star. As the force of gravitational attraction between two bodies is inversely proportional to the square of the distance between the two bodies, the speed at which a living star will move away will increase with the distance which separates it from the superconducting star. Hence the acceleration of the expansion of the universe highlighted by Edwin Hubble. Note also that the further the living stars move away from the extinct superconducting star, the less it is illuminated. Its temperature will therefore decrease as the distances separating it from the living stars increase. In other words, the 2.7 K temperature of superconducting stars measured today thanks to cosmic radiation will continue to drop as the universe expands.

I then present here two scientific observations that can serve as evidence for this new description of the expansion of the universe:

- First, it is impossible for all the dark matter that populates the universe to be lit in exactly the same way to have exactly the same temperature everywhere in the universe. We should therefore observe fluctuations in the intensity of the cosmic radiation in different directions. These fluctuations were first detected in 1992 by the Cosmic Background Explorer Satellite, or COBE, at a level of about one part in a hundred thousand [7].
- Secondly, it is highly probable that the universe today contains superconducting stars which died out first, that is to say before all the others. These stars would be the least illuminated of all and therefore the coldest. Their temperatures should then approach absolute zero and the radiation emitted by these stars would therefore be radio waves. These were discovered in the early 1960s by a group of astronomers led by Martin Ryle at Cambridge. This Cambridge group showed that most of these radiosources must lie outside our galaxy and also that they were many more weak sources than strong ones [7]. Which is quite normal because the universe contains more dark matter than visible matter.

In short, dark matter is therefore made up of stars that have died out and then cooled over time until they become superconducting. They respectively emit microwaves or radio waves when their temperatures are respectively around 2.7 K or close to 0 K. Dark energy is a magnetic repulsive force due to the Meissner effect between superconducting dark matter and the magnetic fields of living stars.

This new description of dark matter and dark energy presented here calls into question two hypotheses supported today by modern cosmology, I quote:

- The existence of a primitive singularity commonly referred to as the “big bang” from which the universe grew to reach the dimensions observed today. The big bang theory is up to now justified by the existence of cosmic radiation at 2.7 K in the microwave range [8]. This radiation is then considered as a signal emitted at a high frequency in the past by the primitive universe then cooled over time to reach us today in the form of a diffuse background in the microwave range. This microwave background is considered to be the only real proof of the veracity of the big bang theory. Thus, if the cosmic radiation is nothing but a simple thermal radiation emitted by cold dark matter, the big bang theory is not supported today by any experimental observation that could serve as proof. We should therefore have some doubts about the veracity of this theory.
- A universe in unlimited or endless expansion. In fact, if the expansion of the universe is due to a Meissner effect between superconducting dark matter and the magnetic fields of stars, this expansion cannot be unlimited; there will surely be an end to the expansion of the

universe. Indeed, the magnetic field of a star is created by dynamo effect. Basically, it is the rotational motion of charged particles in the core of the star that produces this magnetic field. We described this phenomenon of rotation in the Core of the star in an article entitled "The Catastrophe of Rapidly Rotating Fluids", which we published in the "*Open Journal of Applied Sciences*" [10]. Thus, when the star dies, that is to say when it becomes a solid carbonaceous mass, its magnetic field disappears with the dynamo effect. Gravitational attraction then becomes the only force acting between the different extinct stars, the universe contracts and collapses on itself: big crunch [3]. I would still like to underline here the fact that the Bible also alludes to this big crunch in the book of Matthew, I quote: "Immediately after these days of trouble, the sun will darken, the moon will no longer give its light, the stars will fall from heaven, and the powers of the heavens will be shaken" (Matthew 24:29).

4.2 The Einstein Effect

The acceleration of the expansion of the universe described above also has a relativistic effect on the flow of time. This effect, called the Einstein effect, was demonstrated by the physicist Albert Einstein in his theory of general relativity. It can be stated as follows: time passes more slowly when we undergo accelerations [1]. Langevin illustrated the Einstein effect very well in a paradox called "Langevin's twins". In this paradox, he considers two twin brothers who are initially on earth. Then one of the two brothers goes on a space trip for a while. But when he returns to earth, he is surprised to find that his twin brother has become older than him. This "asymmetrical" result is explained by the asymmetry in the changes of reference frames that the two twins underwent: the one who remained on earth, did not change inertial frame of reference, he did not undergo any acceleration. On the other hand, the one who traveled, underwent changes of reference frames of inertia, during accelerations, on takeoff, on arrival on another planet and on landing. Time passes more slowly for the twin brother who has traveled because he has experienced accelerations. The universe being in accelerated expansion, the earth had to undergo many accelerations through time. These accelerations had an effect (the Einstein effect) on the flow of time on our planet. We should therefore be able to observe a significant difference between the measurement of time in the past and the measurement of time today. It is surprising to see how the Bible highlights the Einstein effect in the flow of time on earth. In fact, human life expectancy in the past, as recorded in the book of Genesis, is surprisingly higher than human life expectancy today. I quote for example in the past, Adam who died at the age of 930; Seth who died at the age of 912; Enosch who died at the age of 905; Kenan who died at the age of 910; Mahalaleel who died at the age of 895; Jered who died at the age of 962; Enoch who died at the age of 365; Metuschélah who died at the age of 969; Lemech who died at the age of 777 and Noah who died at the age of 950 (Genesis 5). On the other hand, today, life expectancy in third world countries is 63 years, in the West it is 80 years and the luckiest of men can barely reach 100 years. This huge discrepancy between life expectancy in ancient times and life expectancy today can only be explained by the Einstein effect due to the accelerating expansion of the universe. Because indeed, the scientific progress in medicine carried out today should rather increase human life expectancy instead of decreasing it in a consequent way.

V. CONCLUSION

In this work, we have demonstrated that the theory of evolution in history and the theory of creation in the Bible describe exactly the same events occurring in the same order but it is only the time scales used that differ. The sequence of events in both theories being the same with only one exception, we then matched the times measured by man for each of these events to a proper time measured by God through the relationship of time dilation taken from special relativity. This allowed us to highlight the accelerated expansion of the universe. In this article, we also proposed a new and much more

realistic description of the expansion of the universe. We have shown that this expansion is a phenomenon that simply results from a Meissner effect between superconducting dark matter and the magnetic fields of stars. We also pointed out that this expansion is accelerated because the gravitational force between dark matter and the stars around it decreases as these stars move away from the superconducting dark matter. We have also underlined the relativistic effect of this accelerated expansion of the universe on the flow of time on earth by comparing the human life expectancy in the past as indicated in the book of Genesis and the human life expectancy today.

The book of Genesis dates from a few centuries BC, long before any archaeological excavations and any technologies for dating living beings on earth using Carbon 14. In this article, we have demonstrated and this in a purely scientific way that the first book of the holy Bible is not only a spiritual truth but also a scientific truth, a material reality. The person who took up his brush and wrote word for word the first chapter of this book must have known precisely the discoveries and the results of the archaeological excavations which will be carried out several centuries after him. A being of such superior intelligence that he was able to accurately describe the future of the universe and everything in it. Who else would be this being if not the creator himself?

This study therefore allows us to put an end to the discord that has always reigned between scientists and religious people. Science, with its theory of evolution, in no way contradicts religion, with its theory of creation. On the contrary, the theory of evolution only confirms what is written in the book of Genesis. In other words, science only confirms the existence of God.

REFERENCES

1. Gourgoulhon, E. (2009) General Relativity. Paris Diderot University, Paris.
2. Faure, F. (2002) Introduction to Special Relativity. Joseph Fourier University, Grenoble.
3. Paul, J. and Robert-Esil, J.-L. (2016) The beautiful book of the universe: from the big bang to the big crunch. Dunod, Paris.
4. The Holy Bible (1910) Book of Genesis. Louis second, Paris.
5. Bailly-Bechet, M. (2000) Theory of evolution. University of Yaoundé, Yaoundé.
6. Duloutre, S. (2011) The Acceleration of the Universe. Joseph Fourier University, Grenoble.
7. White, M. and Gribbin, J. (2002) Stephen Hawking a Life in Science. The Joseph Henry Press, Washington D.C.
8. Hawking, S. (2018) Brief Answers to the Big Questions. Bantam Books, New York.
9. Sorongane, E.W. (2022) Quantum Color Theory. *Open Journal of Applied Sciences*, 12, 517-527.https://doi.org/10.4236/ojapps.2022.124036
10. Sorongane, E.W. (2022) The Catastrophe of Rapidly Rotating Fluids. *Open Journal of Applied Sciences*, 12, 469-480. https://doi.org/10.4236/ojapps.2022.124032
11. Sorongane, E.W. (2022) Implementation of a Semi-Classical Theory for Superconductors. *Open Journal of Applied Sciences*, 12, 1243-1253.https://doi.org/10.4236/ojapps.2022.127084